



Orion Racing India Electric

E10

Design Report

Accumulator



Contents

1. System Introduction	6
2. System Goals	6
3. Design Considerations	7
4. System Integration	7
5. Design Estimations	9
6. Lap Simulations	10
7. Configuration & Cell Selection	11
8. Stack Configuration	16
9. Accumulator Design Iterations	17
10. Accumulator Placement Iteration	17
11. Container Iterations	19
12. Lid Design	20
13. Stack Design Flow	21
13.1. Stack Iteration – 1	21
13.2. Stack Iteration – 2	22
14. Plastic vs Metal Stack	23
15. Final Iteration	23
15.1. Boundary condition 1:	24
15.2. Boundary condition 2:	25
15.3. Boundary condition 3:	26
16. Cell Orientation	26
17. Separator Design	27
18. Stack Orientation	28
19. Busbar Design	28
20. Mounting Plate Design	31

21. Final Stack Design	32
22. Insulation	33
23. Manufacturing	34
23.1. Container	34
23.2. Busbar Mounting Plates and Accumulator Mounts	35
23.3. STACK	35
23.4. Assembly	35
24. Accumulator Management System	36
24.1. System goal:	36
24.2. AMS Design.	37
24.3. AMS TOPOLOGY SELECTION.	37
24.4. Slave IC Selection	38
24.5. Master IC Selection	40
24.6. Data Flow through the Accumulator Management System.	41
24.7. Cell temperature monitoring:	42
24.8. AMS Logic Flow Diagram	43
24.9. Model and SoC Estimation:	43
25. Wire Model	45
25.1. Model Verification:	47
26. HV Components	48
26.1. TS Fuse	48
26.2. HV Cables	49
26.3. Maintenance Plugs	49
26.4. Current Sensor	50
26.6. Temperature Sensor	51
27. Future Scope	51

List of Tables

Table 1 : Cell Chemistry Selection	12
Table 2 : Cell Format Comparison	13
Table 3 : Cell Model Comparison	14
Table 4 : Accumulator Characteristic	16
Table 5 : (a) Accumulator Placement Iterations	18
Table 6 : Lid Design Iterations Comparison	20
Table 7 : Property data	24
Table 8 :Properties of standard grades of copper and aluminium	30
Table 9 : AMS Slave Monitoring IC Selection	39
Table 10 : AMS Master IC Selection	40

List of Figures

Figure 1 : Complete accumulator CAD	6
Figure 2 : System Goals	6
Figure 3 : Overview of Design Flow of Accumulator	7
Figure 4 : Ergonomics and packaging considerations in design (Block-CAD)	8
Figure 5 : Side Profile of Accumulator as mounted on car	8
Figure 6 : Performance Comparison	9
Figure 7 : Energy Consumption VS Torque & Energy Consumption VS Weight	10
Figure 8 : Battery consumption VS Coefficient of Drag	11
Figure 9 : Cell Selection Procedure & Sensitivity of Energy Consumption to different Vehicle Parameters	11
Figure 10 : Cell Format Comparison	13
Figure 11 : Cell Comparison graph	14
Figure 12 : Excel workbook for all cells analyzed	15
Figure 13 : Cell Data	15
Figure 14 : a) Accumulator Behind Seat b) Accumulator in sidepods	17
Figure 15 : Cg and moment of inertia values	18
Figure 16 : Accumulator Block CAD	19
Figure 17 : Cell Placement inside Accumulator (1 column of 34 cells)	19
Figure 18 : Cell Placement inside Accumulator (2 row of 17 cells each)	20
Figure 19 : Lid CAD Design	21
Figure 20 : Stack Design Flow	21
Figure 21 : CAD of Stack Iteration - 1	22
Figure 22 : Stack stress evolution as a function of cycle number	22
Figure 23 : CAD of Stack Iteration - 2	23
Figure 24 : Plastic vs Metal Stack	23
Figure 25 : Final Iteration Stack CAD	24
Figure 26 : Simulation for boundary condition 1	25
Figure 27 : Simulation for boundary condition 2	26

Figure 28 : Simulation for boundary condition 3	26
Figure 29 : 2p17s Stack Configuration (Busbar Schematic)	27
Figure 30 : CAD of Separator Placement	27
Figure 31 : (a) Schematic of electrical connections of 6 stacks (b) CAD rendering of Electrical connection	
28	
Figure 32 : Overlapped Cell Tabs between Busbar and FR4	28
Figure 33 : Comparison of Aluminium and Copper	29
Figure 34 : Busbar Material Ratings	30
Figure 35 : Top View of Stack	31
Figure 36 : Mounting Plate Selection	32
Figure 37 : Cell Holder CAD	32
Figure 38 : One Stack CAD	33
Figure 39 : Comparison of Insulation Material	33
Figure 40 : Container Fixture	34
Figure 41 : Stack Exploded View	36
Figure 42 : AMS System Goal	36
Figure 43 : AMS Design Flow	37
Figure 44 : AMS Topology Selection	38
Figure 45 : Modular AMS Topology	38
Figure 46 : Slave PCB	39
Figure 47 : Master PCB	40
Figure 48 : Data flow diagram	41
Figure 49 : NTC Placement	42
Figure 50 : AMS Logic Flow Diagram	43
Figure 51 : Simulink Model	44
Figure 52 : SOC Curve	44
Figure 53 : Simulation Graph	45
Figure 54 : Wire Model Flowchart	46
Figure 55 : Simulink Wire Model	47
Figure 56 : Input Parameters	47
Figure 57 : Working Model for 25mm squared wire	48
Figure 58 : TS Fuse Datasheet	48
Figure 59 : Helu Kebel 25mm ² datasheet	49
Figure 60 : Maintenance Plug Datasheet	50
Figure 61 : Current Sensor	50
Figure 62 : Accumulator Isolation Relay	50
Figure 63 : Temperature Sensor	51
Figure 64 : Composite Accumulator	51

1. System Introduction

The Accumulator of an Electric Vehicle is one of the fundamental components of an Electric Vehicle Powertrain, alongside the Motor and Motor Controller. The Tractive System Accumulator consists of a complex assembly of electrical cells, monitoring electronics and protection systems. Electrical Cells, due to their sensitive and fragile nature, requires precise structural support and electronic management. For a Formula Student Electric Vehicle, the accumulator design has a direct impact on overall vehicle performance, since it controls the amount of energy available at the disposal of the vehicle for propulsion, as well as how that energy is delivered. The accumulator design also has an impact on the mechanical characteristics of the vehicle, since it directly affects packaging, cooling and dynamics.

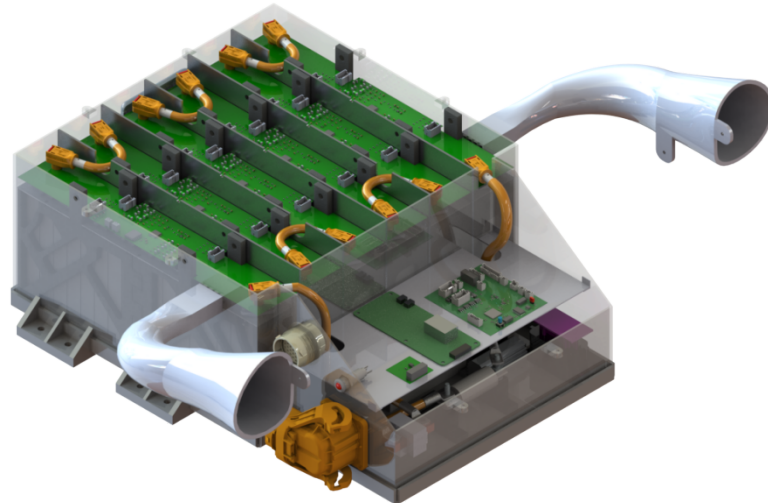


Figure 1: Complete accumulator CAD

The Accumulator Management System is responsible for measuring and monitoring all cell voltages and temperature and also the TS current, if any of these parameters go beyond the specified range then give a fault signal which shuts down the vehicle while running or during the charging process. It is also capable of communicating with the data logger to store the data from the accumulator to be viewed later and analyze it for validation and future references.

2. System Goals

The system goals were decided such that they align the mindset of the members directly with the team goal to ensure that the system is designed with the overall vehicle and its performance and safety in mind.

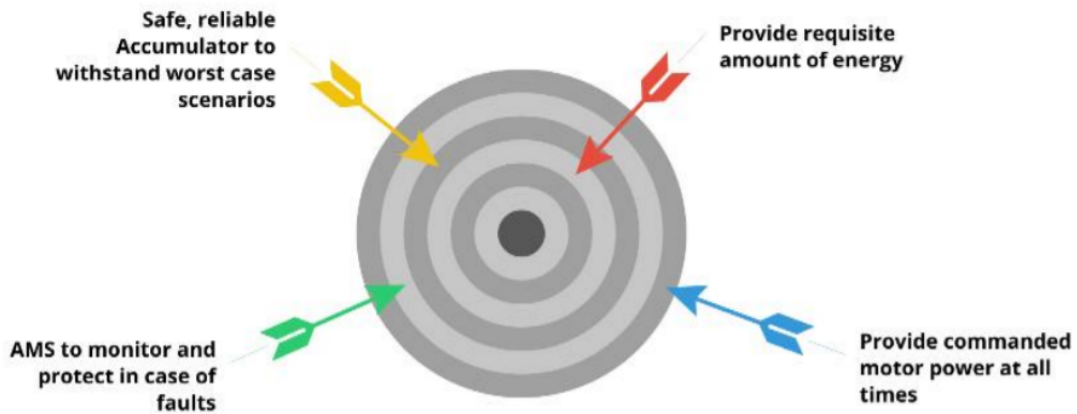


Figure 2: System Goals

3. Design Considerations

The design of the accumulator began keeping the chassis as a reference. This helped in setting constraints for cell and container dimensions.

1. It was considered that the accumulator should be able to deliver the maximum motor power at all times, hence the ratings of the cells were to be chosen appropriately.
2. The heat output of the cells during continuous discharge would influence the design of the container, and adequate cooling provisions would have to be made.
3. Since the discharge characteristics of the cells were not known completely at the beginning of the design phase, a large Factor of Safety (FoS) was taken in the ratings and design of the accumulator.
4. For computation and simulation purposes, the weight of the vehicle was assumed to be 208KG, and the weight of the driver was assumed to be 65 KG, which brings the total weight to 273 KG.

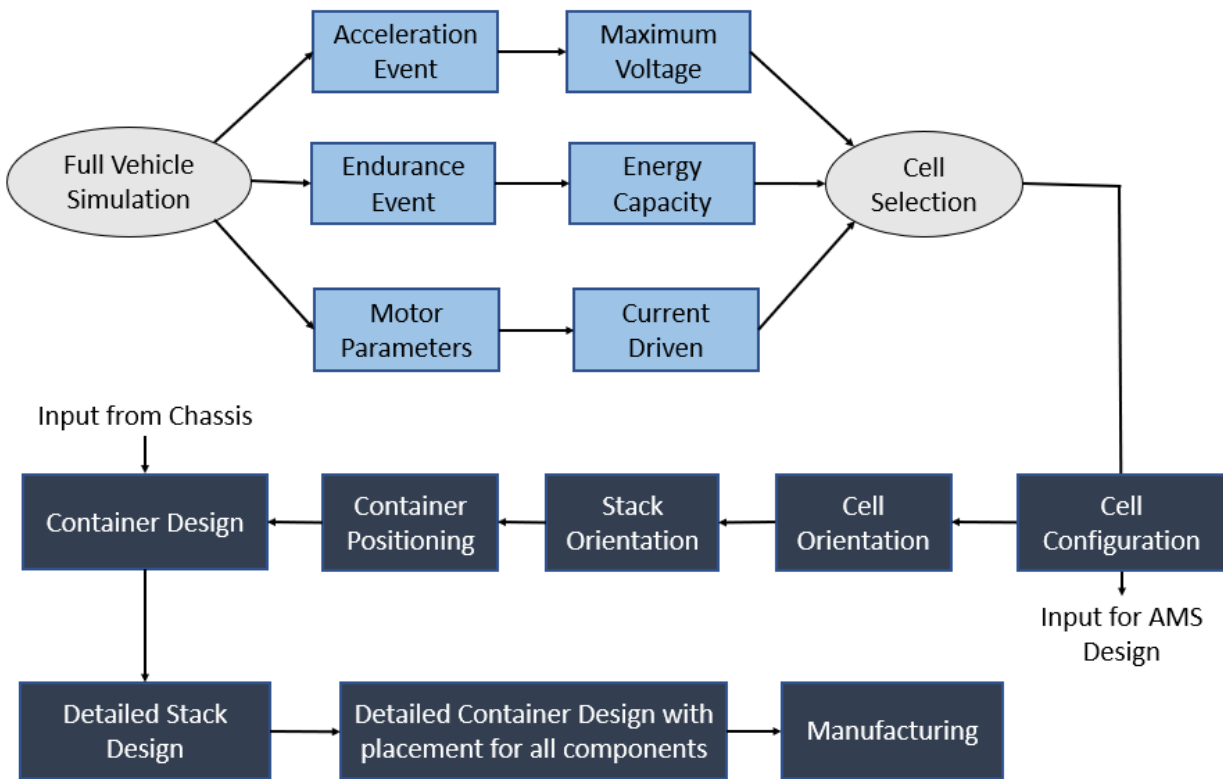


Figure 3: Overview of Design Flow of Accumulator

4. System Integration

The accumulator is one of the critical components of the vehicle, and complete integration of it into the overall vehicle design is essential. A holistic approach to vehicle design, that takes into consideration the interrelationships between systems are key to designing a high-performance, reliable vehicle. In that view, the systems affected by accumulator design, and the impact thereon, is presented as follows:

- Ergonomics and Packaging: In order to maximise available volume, as well as keep the centre of gravity as close to the centre as possible, the accumulator container was designed with a sloping face. The angle of the slope matches the incline of the drivers' seat, thus allowing the accumulator container to move further forward, releasing space for the motor and drivetrain behind it. Also, the Low Voltage Battery shares space in the same inclined area, further improving packaging.

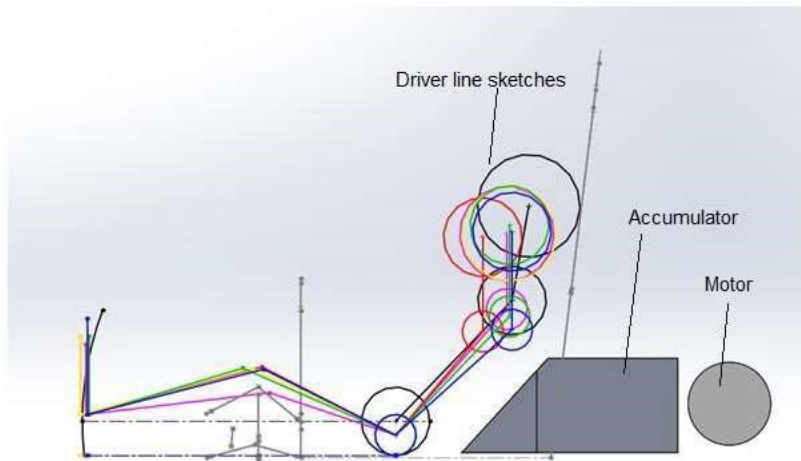


Figure 4: Ergonomics and packaging considerations in design (Block-CAD)

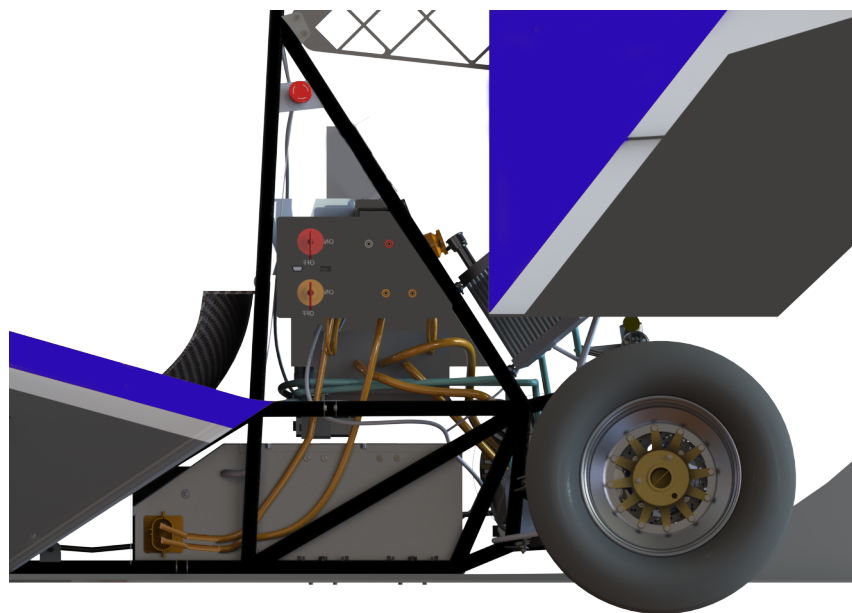


Figure 5: Side Profile of Accumulator as mounted on car

- Vents on the side of the container are provided for ventilation to prevent any accumulation of gases according to the rules. The placement of these vents was done with chassis tubes' position in mind.
- Suspension: Placing the large accumulator container affects suspension kinematics, as the suspension points get pushed outward.
- Electronics: Integration of Low Voltage (LV) systems with the AMS was done for the logging of cell parameters, such as voltage, temperature and current. Additionally, the AMS Master was interfaced with the CAN network for communication with the accumulator charger.

5. Design Estimations

Considering the lack of practical data due to Covid-19 induced lockdowns, the decision-making process for most of the parameters of the battery pack relied on data from lap simulations. Simulations were run for each event multiple times on Formula Bharat's Track, and the data gathered from them was used to decide the pack parameters. Each event gave us data for a different parameter.

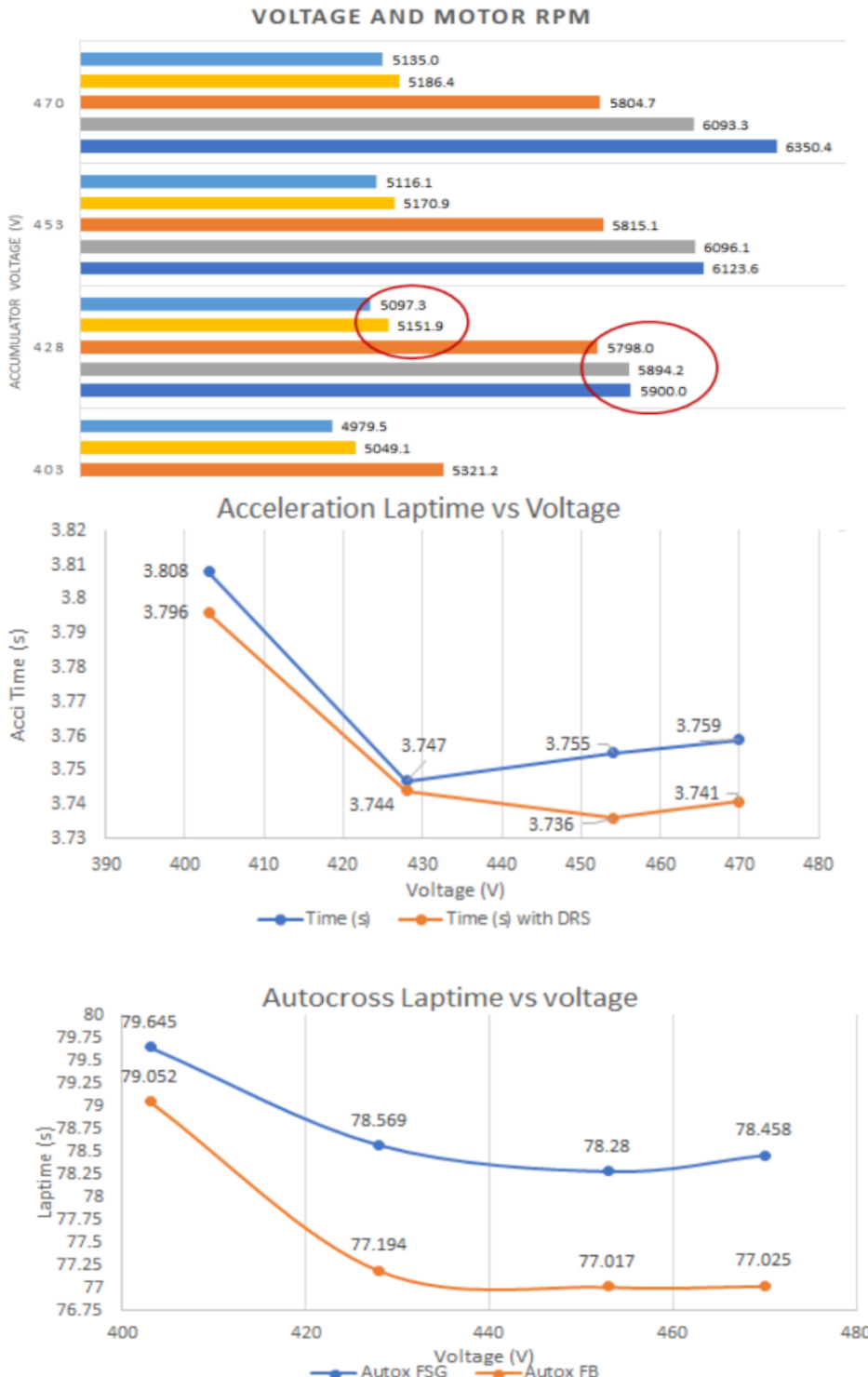


Figure 6: Performance Comparison

From this figure, the maximum motor RPM achieved was 5900 RPM. The motor datasheet specifies a range from 11 to 14 RPM / Volt depending on the load. Hence, an average case of load was considered to maximize RPM swing. Thus, converting the RPM values, we get a terminal pack voltage of 421.4 V.

6. Lap Simulations

The maximum voltage of our motor is 470V and thus we tried to go as close as possible to increase the efficiency of the system and looking at all the constraints a 2p102s configuration was chosen which was the best possible configuration leading to the accumulator voltage of 428.4 and the energy capacity was 7.2 KWh. The maximum value of current discharge was found to be approximately 240A. However, the values obtained from lap simulators often do not match with practical.

Using these values for current and voltage, simulations were run using varying different parameters to make a sensitivity analysis, by changing aero configuration, weight and torque for example. The effect of these variations on the final energy consumption for an endurance track was studied. 6.9KWh was obtained to be energy energy consumption during endurance.

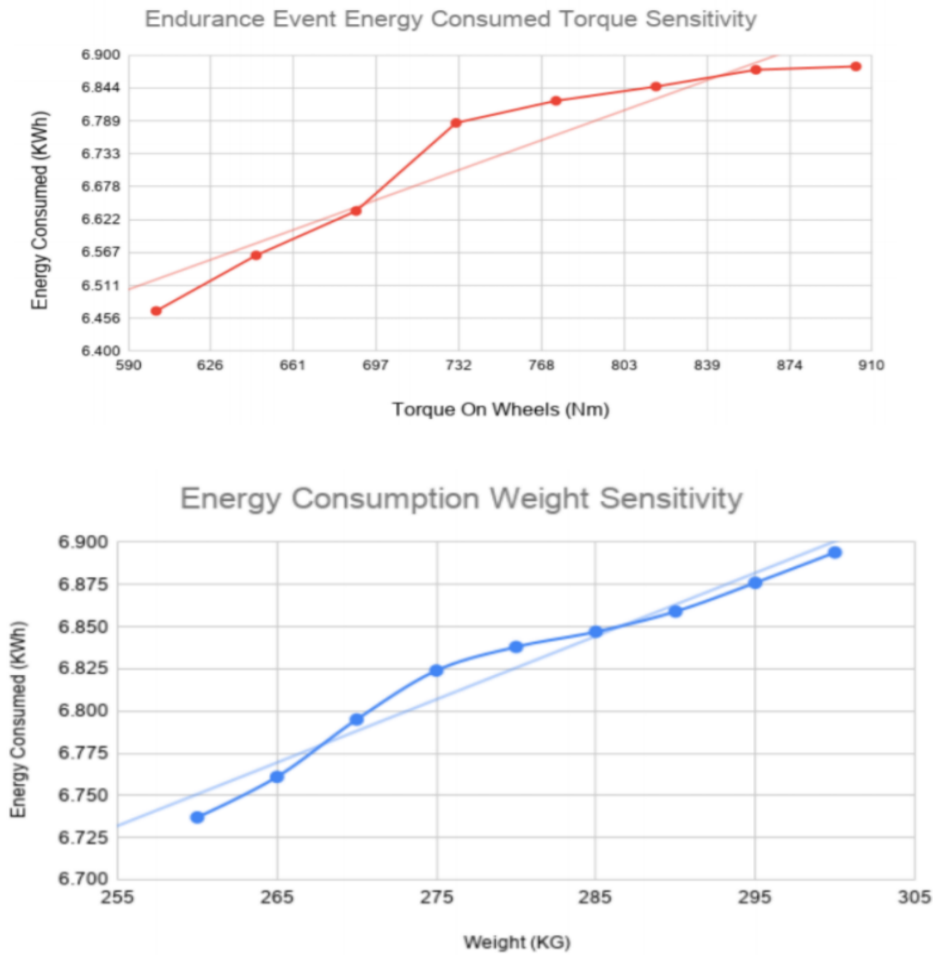


Figure 7: Energy Consumption VS Torque & Energy Consumption VS Weight

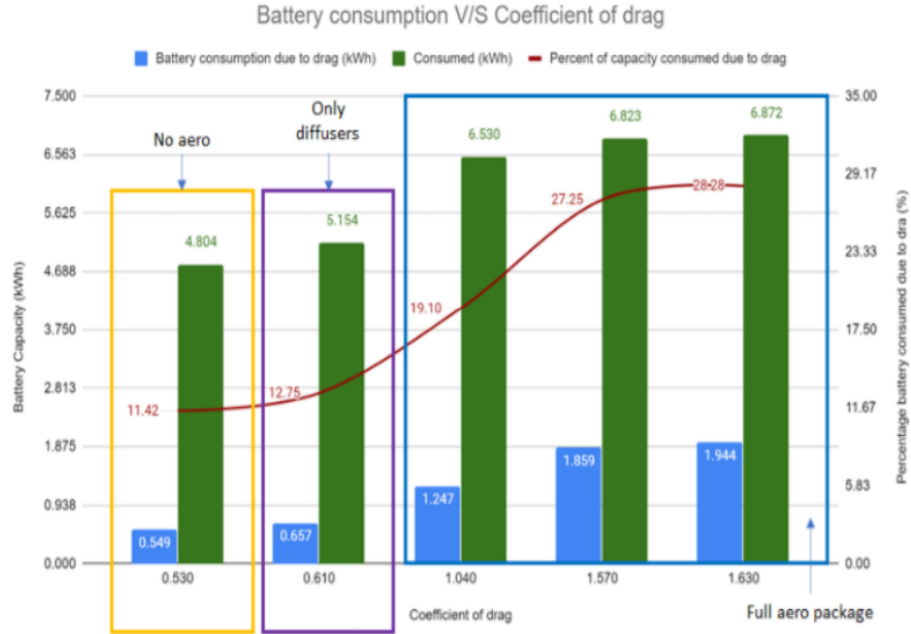


Figure 8 : Battery consumption VS Coefficient of Drag

Practical conditions tend to differ from simulator conditions, since simulators assume ideal conditions. Perfectly flat tracks, consistent driving styles and constant ambient conditions are some of the assumptions made by the simulator. To compensate for this difference, a factor of safety must be added to the value given by the simulator. In the previous year, the team had overestimated the factor of safety for energy consumption and thus had over designed the accumulator. This year the team decided to go with a smaller margin and decided to fix the energy capacity at around 7.2 KWh.

7. Configuration & Cell Selection

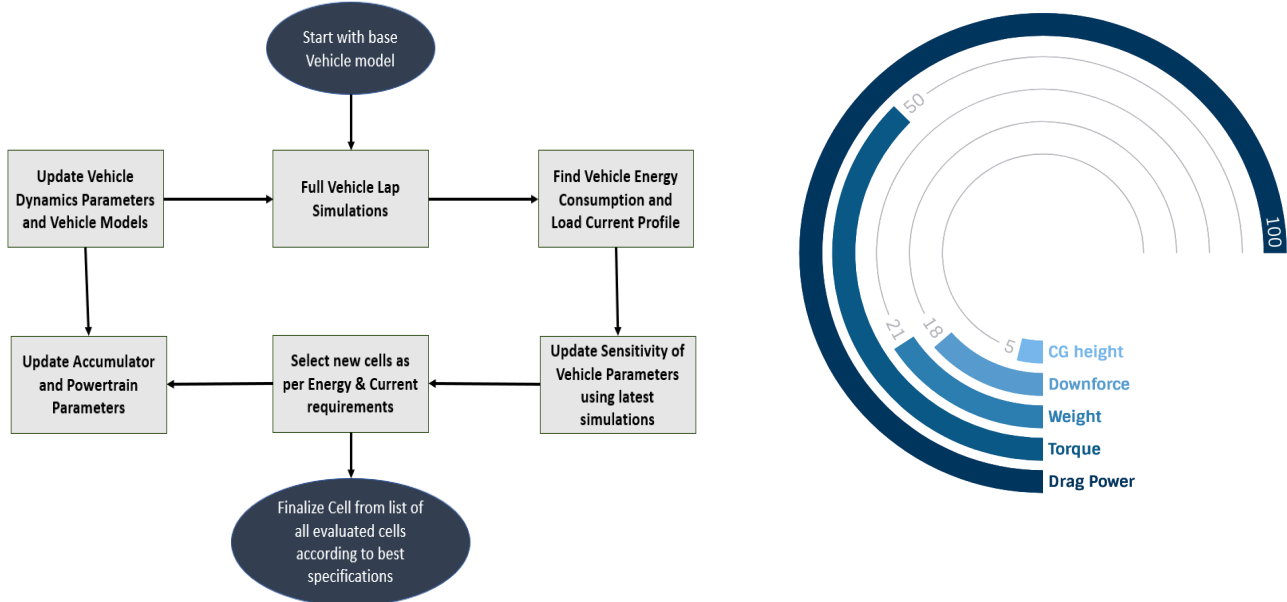


Figure 9: Cell Selection Procedure & Sensitivity of Energy Consumption to different Vehicle Parameters

Cell selection stands as one of the most important procedure while deciding the accumulator parameters and a cell model which can parameterize an equivalent circuit model using the lab test data was made and the charging and discharging characteristics of the cell along with the SOC vs OCV curve at different discharge currents are as shown and amongst the cylindrical and pouch cells. The decision was taken with the help of a decision matrix that incorporated the parameters like energy density, max current, internal resistance, capacity, etc. By observing the simulation data generated, the required parameters for the cell were computed keeping in mind these parameters as a factor of priority Cell selection was performed. The selection procedure started with identifying the best cell chemistry for the application, followed by the structure or format, and then narrowed down to the individual model.

The following table presents a comparison between different cell chemistries suitable for high power applications, such as an electric vehicle. The parameters considered are Voltage, Energy Density, and Current Delivery capabilities amongst others.

Parameters	Lithium Manganese Oxide	Lithium Phosphate	Iron	Lithium Cobalt Oxide
Nominal Voltage (V)	3.8	3.2		3.7
Maximum Voltage (V)	4.3	3.6		4.2
Gravimetric Energy Density (Wh / Kg)	~120	~110		~180
Current Delivery capability	Lower than other two	High		High
Coulombic Efficiency	~90%	~95%		~90%
Lifecycles	500-1000	>2000		<500
Available Formats	Cylindrical	Cylindrical, Flat Pouch, Prismatic		Cylindrical, Flat Pouch, Prismatic

Table 1: Cell Chemistry Selection

From our research, we found that Lithium Cobalt Oxide (LiCoO₂) cells have higher nominal voltage and gravimetric energy density as compared to other chemistries. It has lower lifecycle count and slightly lower efficiency as compared to other chemistries, but the higher energy density and current draw outweigh these drawbacks, hence making LiCoO₂ cells the choice for the accumulator.

Other Nickel-based chemistries such as NiMH and NiCad were considered as well, but their low nominal voltage and correspondingly low energy density made them a poor choice for a high-power battery pack.

The next step is selection of the cell format. The main formats considered were cylindrical, flat pouch and prismatic. The main factors looked at were packaging efficiency, availability of cells, as well as mechanical

constraints such as cooling possibilities and ease of manufacturing. Also, to save weight, it is imperative that a minimum number of cells are placed in parallel that satisfy current requirements. Also, maximum energy density was desired so as to reduce weight further.

Parameters	Lithium Manganese Oxide	Lithium Iron Phosphate	Lithium Cobalt Oxide
Nominal Voltage (V)	3.8	3.2	3.7
Maximum Voltage (V)	4.3	3.6	4.2
Gravimetric Energy Density (Wh / Kg)	~120	~110	~180
Current Delivery capability	Lower than other two	High	High
Coulombic Efficiency	~90%	~95%	~90%

Table 2: Cell Format Comparison

Cell Format Comparison

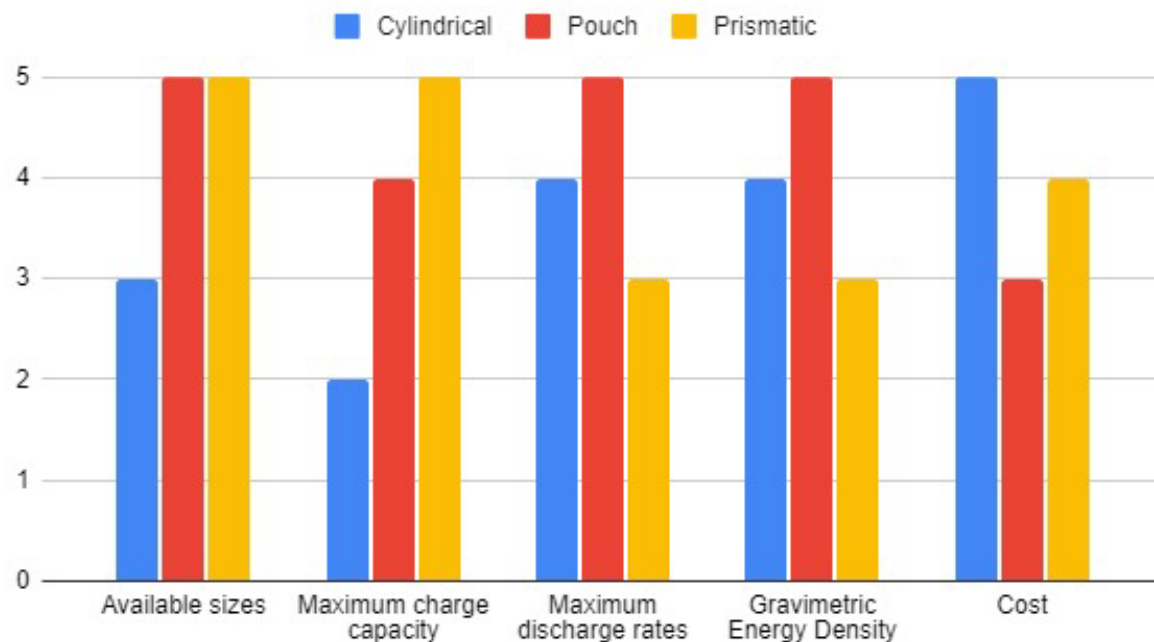


Figure 10: Cell Format Comparison

After performing market research, we found that flat pouch cells satisfy all the above requirements. Cylindrical cells do not have sufficient current delivery capability and thus require parallel strings of cells, which add weight and manufacturing difficulty. Flat pouch cells are available in much higher varieties of capacity and current draw, and thus offer the flexibility to fit into any design.

Model	Capacity (Ah)	Discharge Rate (C)	Weight (g)	Internal Impedance ($\text{m}\Omega$)	Dimensions (L x B x T) (mm)
L1174170	16	15	393.5	1.1	189.5 x 89.5 x 10
YIS-HEDK885155	16.8	15	313.5	1.2	154.5 x 85 x 10.5
Melasta SLPBA390190	16	10	283	1.5	189.5 x 89.5 x 10
Melasta SLPBA347145	8.4	15	152	1.2	145 x 47 x 10

Table 3: Cell Model Comparison

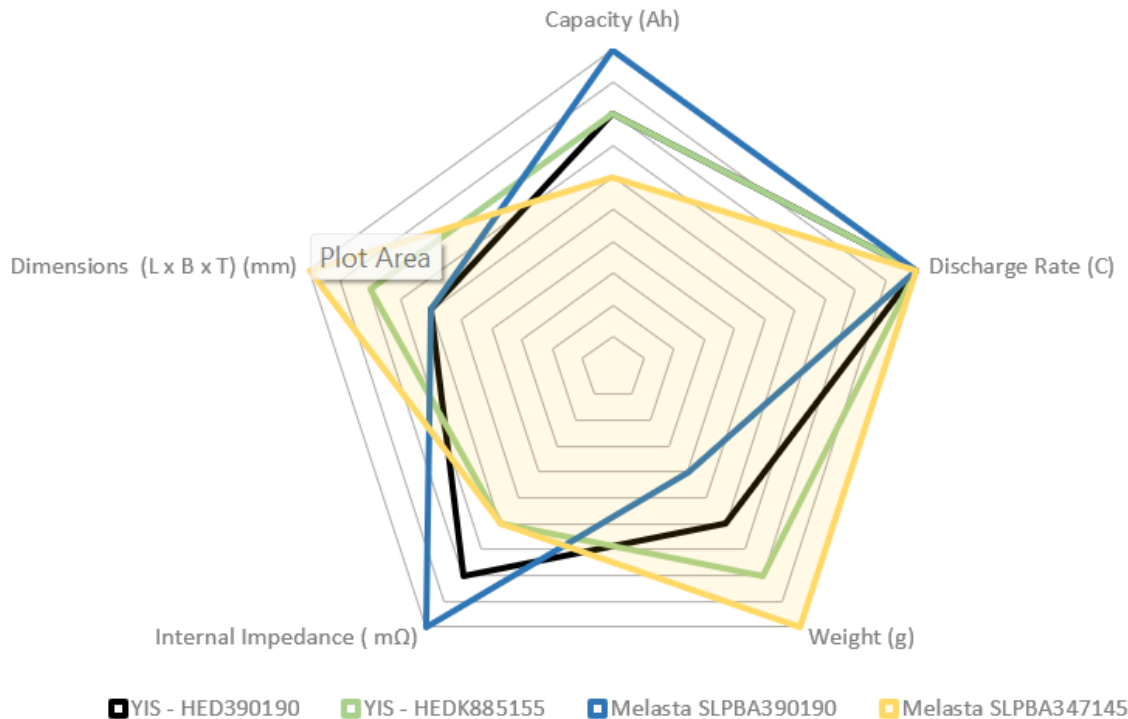


Figure 11: Cell Comparison graph

Max Continuous Charge Rate	Max Continuous Discharge Rate	Nominal Voltage	Charge Voltage	Capacity	The Max Discharge Current of the Cell	Weight	Impedance	Cells' Dimensions (mm)	Distance between Two Tabs (mm)	Standard Size of Tabs (mm)			Sealing Width (mm)	current	pack voltage	number of cells	energy	raw weight	max pack discharge current	pack impedance	volume	energy density	floor area					
										L	W	T																
SLPB9345135	10A	15	3.7V	42	6100	120	119.0	1.3	135.5	45.0	8.8	20±1	LCO	10.0±1.0	15	0.2	5.0±0.2	183	428	102	5.22648	24.776	240	66.3	107.316	0.23873	215.294	80784
SLPB7564159	10A	20	3.7V	42	7500	160	157.0	1.1	158.5	63.5	7.1	29±1	LCO	10.0±1.0	20	0.2	8.3±0.2	300	428	102	6.426	32.028	320	56.1	142.919	0.2204	200.637	9173.4
SLPB7364159	10A	20	3.7V	42	7500	160	154.0	0.9	158.5	64.0	7.0	29±1	LCO	10.0±1.0	20	0.2	8.3±0.2	300	428	102	6.426	31.416	320	45.9	142.016	0.22181	204.345	91392
SLPB8863124	10A	15	3.7V	42	7500	160	148.0	1.1	126.0	63.0	8.1	30±1	LCO	10.0±1.0	20	0.2	5.0±0.2	225	428	102	6.426	30.192	320	56.1	128.596	0.24495	212.838	104101
SLPB88463124	10A	15	3.7V	42	7500	160	148.0	1.1	126.0	63.0	8.1	30±1	LCO	10.0±1.0	20	0.2	5.0±0.2	225	428	102	6.426	30.192	320	56.1	128.596	0.24495	212.838	104101
SLPB88663124	10A	15	3.7V	42	7500	160	149.5	1.1	126.0	63.0	8.2	30±1	LCO	10.0±1.0	20	0.2	5.0±0.2	225	428	102	6.426	30.498	320	61.2	130.183	0.24197	210.702	105386
SLPB88663124	10A	15	3.7V	42	7500	160	149.5	1.1	126.0	63.0	8.3	30±1	LCO	10.0±1.0	20	0.2	5.0±0.2	225	428	102	6.426	30.498	320	56.1	131.771	0.23903	210.702	106172
SLPB8863124	10A	15	3.7V	42	7500	160	153.0	1.2	126.0	63.0	8.4	30±1	LCO	10.0±1.0	20	0.2	5.0±0.2	225	428	102	6.426	31.212	320	61.2	133.358	0.23621	205.882	107957
SLPB9095100	10A	25	3.7V	42	8000	280	172.0	0.8	99.0	94.5	8.7	50±1	LCO	10.0±1.0	35	0.2	8.3±0.2	400	428	102	6.8544	35.088	560	40.8	162.788	0.20641	195.349	167719
SLPB9095100	10A	25	3.7V	42	8000	280	172.0	0.8	99.0	94.5	8.7	50±1	LCO	10.0±1.0	35	0.2	8.3±0.2	400	428	102	6.8544	35.088	560	40.8	162.788	0.20641	195.349	167719
SLPB88659156	10A	30	3.7V	42	8000	160	168.0	0.8	156.0	58.5	8.2	29±1	LCO	10.0±1.0	20	0.2	5.0±0.2	480	428	102	6.8544	34.272	320	40.8	149.666	0.2245	200	97858.8
SLPB7664155	10A	20	3.7V	42	8000	160	155.0	0.9	155.0	63.5	7.3	29±1	LCO	10.0±1.0	20	0.2	5.0±0.2	320	428	102	6.8544	31.162	320	45.9	143.701	0.23382	216.774	94564.2
SLPB7664155	10A	15	3.7V	42	8000	144	156.0	1.3	155.0	63.5	7.3	29±1	LCO	10.0±1.0	18	0.2	5.0±0.2	240	428	102	6.8544	31.824	288	66.3	143.701	0.23382	215.385	94564.2
SLPB88459156	10A	30	3.7V	42	8000	160	166.0	1.0	156.0	59.0	8.1	29±1	LCO	10.0±1.0	20	0.2	5.0±0.2	480	428	102	6.8544	33.864	320	51	149.105	0.22534	201.41	97491.6
SLPB7864155	10A	15	3.7V	42	8000	144	162.0	1.1	155.0	64.0	7.2	29±1	LCO	10.0±1.0	18	0.2	5.0±0.2	240	428	102	6.8544	33.048	288	56.1	142.848	0.23522	207.407	94003.2
SLPB88364155	10A	20	3.7V	42	8000	160	167.0	0.9	155.0	64.0	7.6	29±1	LCO	10.0±1.0	20	0.2	5.0±0.2	320	428	102	6.8544	34.068	320	45.9	151.277	0.22212	201.198	99225.6
SLPB90959156	10A	30	3.7V	42	8000	160	173.0	0.8	156.5	59.0	8.3	29±1	LCO	10.0±1.0	20	0.2	5.0±0.2	480	428	102	6.8544	35.292	320	40.8	153.276	0.21921	194.22	99888.8
SLPB9090092	10A	15	3.7V	42	8000	144	160.5	1.3	91.5	90.0	9.4	35±1	LCO	10.0±1.0	18	0.2	8.3±0.2	240	428	102	6.8544	32.742	288	66.3	154.818	0.21703	209.346	172584
SLPB88164155	10A	20	3.7V	42	8000	160	172.0	1.1	155.0	64.0	7.7	29±1	LCO	10.0±1.0	20	0.2	5.0±0.2	320	428	102	6.8544	35.088	320	51	152.768	0.21994	195.349	100531
SLPB88164155	10A	15	3.7V	42	8000	144	162.5	1.1	91.5	90.0	9.5	35±1	LCO	10.0±1.0	18	0.2	8.6±0.2	240	428	102	6.8544	33.115	288	56.1	156.463	0.21747	206.769	174462
SLPB88164155	10A	20	3.7V	42	8000	160	171.5	0.8	158.5	64.0	7.7	29±1	LCO	10.0±1.0	20	0.2	8.6±0.2	320	428	102	6.8544	34.986	320	40.8	156.218	0.21938	195.918	100531
SLPB89159156	10A	30	3.7V	42	8000	160	178.0	0.8	156.5	59.0	8.8	29±1	LCO	10.0±1.0	20	0.2	5.0±0.2	480	428	102	6.8544	36.312	320	40.8	162.51	0.20676	188.764	105917
SLPB9259156	10A	30	3.7V	42	8000	160	178.0	0.8	156.5	59.0	8.8	29±1	LCO	10.0±1.0	20	0.2	5.0±0.2	480	428	102	6.8544	36.312	320	40.8	162.51	0.20676	188.764	105917
SLPB6045270	10A	10	3.7V	42	8300	120	160.0	1.4	270.0	45.0	5.8	22±1	LCO	10.0±1.0	15	0.2	5.0±0.2	166	428	102	7.11144	37.64	240	71.4	140.94	0.24774	217.875	5344
SLPB8847145	10A	15	3.7V	42	8400	120	152.0	1.2	145.0	47.0	10.0	25±1	LCO	10.0±1.0	15	0.2	5.0±0.2	252	428	102	7.19712	31.008	240	61.2	136.3	0.25884	232.105	95880
SLPB8572196	10A	8	3.7V	42	8900	96	165.0	1.4	195.5	72.0	5.3	26±1	LCO	10.0±1.0	12	0.2	5.0±0.2	142.4	428	102	7.62552	33.66	192	71.4	149.206	0.25053	226.545	77846.4
SLPB86072196	10A	8	3.7V	42	8900	96	169.0	1.4	196.0	72.5	5.3	26±1	LCO	10.0±1.0	12	0.2	5.0±0.2	142.4	428	102	7.62552	34.476	192	71.4	150.626	0.24816	221.183	78387

Figure 12: Excel workbook for all cells analyzed

From the simulation data, the required parameters of the cell were computed. These required parameters are as follows:

Charge Capacity required:>16.2Ah

Discharge Rate: > 240 A continuous

Additionally, the internal impedance, weight and dimensions of the cells were prioritized in order respectively. From the above parameters, we selected the Melasta SLPB8847145 Lithium Polymer cell as it met all the requirements. Additionally, it has a very low internal impedance of 1.2 mΩ, which ensures low thermal losses in the cell, and higher power delivery capability. For implementation of regenerative braking, cells selected needed to have reasonably high charging rates. Hence the team decided to go with 2 cells in parallel. The final configuration has 2 parallel strings of cells, resulting in a 2p102s configuration.

◆ 电芯正极材料 Cell Cathode Material	LiCoO2	
◆ 标称容量 Typical Capacity①	8400mAh	
◆ 标称电压 Nominal Voltage	3.7V	
◆ 充电条件 Charge Condition	Max. Continuous charge Current	16.8A
	Peak charge current	25.2A(\leq 3sec)
	Voltage	4.2V \pm 0.03V
◆ 放电条件 Discharge Condition	Max Continuous Discharge Current	120A
	Peak Discharge Current	168A(\leq 3sec)
	Cut-off Voltage	3.0V
◆ 交流内阻 AC Impedance(mΩ)	1.2 \pm 0.2	
◆ 循环寿命【充电:0.5C,放电:120A】 Cycle Life 【CHA:0.5C,DCH:120A】	>100cycles	

Figure 13: Cell Data

Attribute	Value	Unit
Maximum Accumulator Voltage	428.4	V
Nominal Accumulator Voltage	377.4	V
Maximum Accumulator Energy	7.19	KWh
Nominal Accumulator Energy	6.34	KWh
Continuous discharge current	252	A
Charge Capacity	16.8	Ah
Cell Configuration	2p102s	-
Overall Weight	50	Kg
Energy Density	160	Wh/Kg

Table 4: Accumulator Characteristic

8. Stack Configuration

From the simulation data, the maximum voltage required from the accumulator was 428.4 V, and the energy required was > 7 KWh. The selected cell chemistry, Lithium Cobalt Oxide, has a peak cell voltage of 4.2 V. Hence, the number of cells required was computed as:

$$\text{Total Voltage of Accumulator} / \text{Peak Voltage of Cell} = \text{Number of Cells in Series}$$

$$428.4 / 4.2 = 102$$

Hence the number of cells chosen in series is 102 and the overall configuration of the pack is 2p102s

The maximum voltage of the accumulator is $4.2 \times 102 = \mathbf{428.4 \text{ V}}$. The nominal voltage of the accumulator is $3.7 \times 102 = \mathbf{377.4 \text{ V}}$

For the selected cell, the nominal and peak energy was computed by multiplying the charge capacity of the pack (charge capacity of cell x No. of parallel combination) with the nominal and maximum voltages of the accumulator respectively.

Hence, the nominal energy of the pack is $377.4 \times 8.4 \times 2 = 6.34 \text{ KWh}$ The maximum energy of the pack is $428.4 \times 8.4 \times 2 = \mathbf{7.19 \text{ KWh}}$

According to EV 5.3.2, the accumulator must be divided into segments, with each segment having a terminal voltage not exceeding 120V and energy not exceeding 6 MJ. From this rule, the maximum number of cells that can be accommodated in one segment is computed as:

$$\text{Number of cells in segment} = \text{Maximum Energy per Segment} / \text{Maximum Energy per Cell}$$

$$\begin{aligned}
 &= 6\,000\,000 / (4.2 \times 8.4 \times 3600) \\
 &= 47.24 \quad \sim \mathbf{47}
 \end{aligned}$$

However, we decided to keep the number of cells in a segment constant, in order to simplify the design of the AMS slaves and the container. Hence, we decided to keep the number of cells per segment equal to 34, as the pack of 204 cells can be equally divided into 6 segments.

Hence, the energy of each segment is computed as:

$$\begin{aligned}
 \text{Energy of Segment} &= \text{Maximum voltage of segment} * \text{Charge Capacity of Segment} \\
 &= 4.2 * 17 * 8.4 * 2 * 3600 \\
 &= \mathbf{4.318 \text{ MJ}}
 \end{aligned}$$

9. Accumulator Design Iterations

The initial design had started with a rough cell calculation and selection which was assumed for making the block CAD of the accumulator. Also feedback from previous year designs was used to get an approximation of cell gap required for cooling and conduction.

This helped us develop a sample stack model which was used to approximate the size of the accumulator, its weight and position on the vehicle. These iterations were done keeping in mind the following considerations along with keeping the FSE rules in mind while designing:

- The spacing would be around 10.6 mm between cell faces.
- The AMS would be connected by using ring terminals and a connection and would be compact enough to fit on top of the cells.
- The weight of each stack would be about 6 kg each.
- The net weight would be 50 kg.

10. Accumulator Placement Iteration

Before deciding the stack orientation and placement, it was essential to finalize the placement of the accumulator on the vehicle. Hence, the following placements were considered:

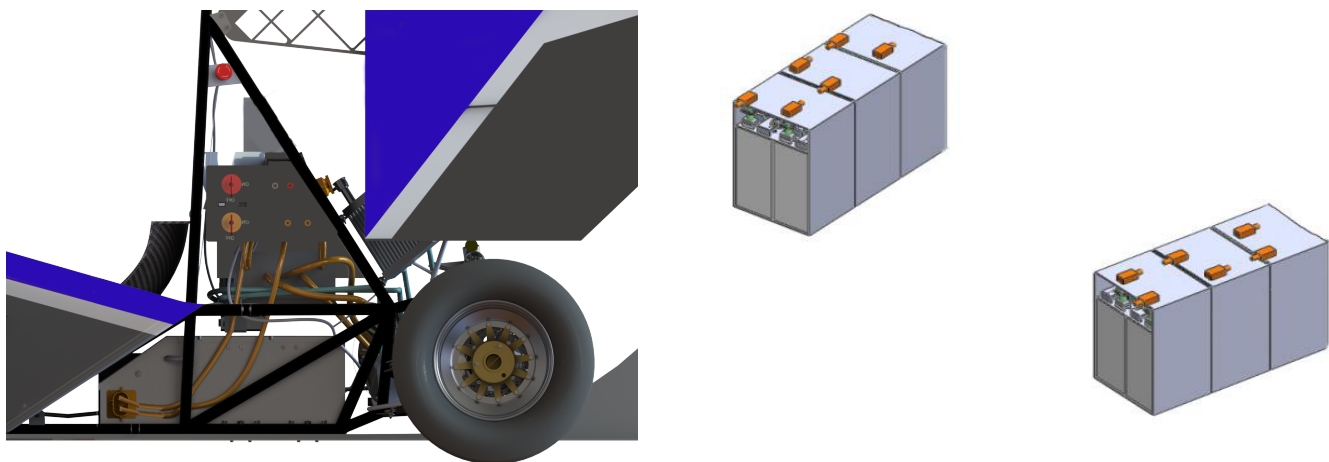


Figure 14: a) Accumulator Behind Seat b) Accumulator in sidepods

Parameters	Iteration 1	Iteration 2
Description	Accumulator behind the seat	Accumulator in sidepods
Ergonomics	More flexible	Similar
Cooling	Difficult	Better
Vehicle Dynamics	Better (Closer to CG and hence lower roll and yaw inertias)	Worse (Higher mass away from CG)
Electronics	Better (lesser components)	Worse (Greater components as accumulator split into two parts)
Packaging & accessibility	Worse (influences packaging heavily)	Better (more flexibility for drivetrain and chassis)
Chassis	Can be lighter as accumulator easily fits into impact structure	Has to integrate a separate impact protection structure
Weight	Lighter	Heavier

Table 5: (a) Accumulator Placement Iterations

		Final Iteration	Sidepod Iteration
CG	X	0	0
	Y	777	702.783
	Z	278	312.1
MOI (kgm^2)	I_{yy} (Roll)	20.395	43.374
	I_{zz} (Yaw)	79.817	101.941



Figure 15: Cg and moment of inertia values

11. Container Iterations

Earlier it was decided that the accumulator will be an T - shaped one with a rectangular cross-section. This design was further iterated in the vehicle block cad; following were the points that were not favourable:

- The length of the accumulator was large enough, such that the wheelbase had to be significantly increased for packaging of the powertrain
- There was a lot of space vacant under the seat which was not favourable

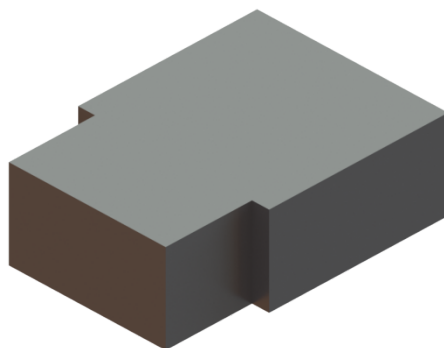


Figure 16: Accumulator Block CAD

To better package the accumulator, the front portion was made with a slanting face which could fit below the seat.

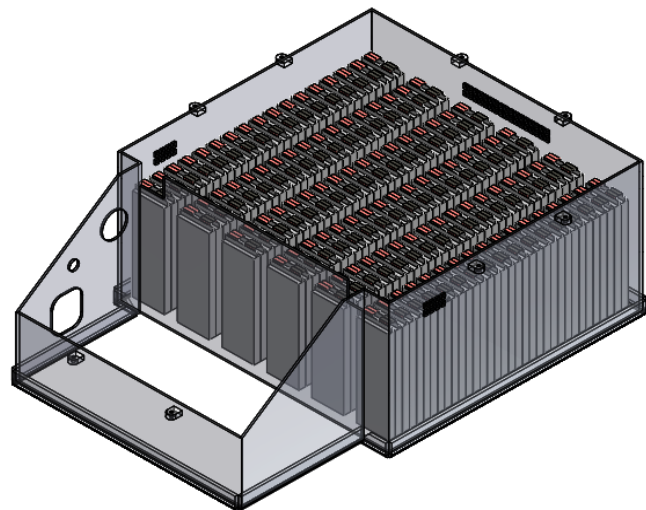


Figure 17: Cell Placement inside Accumulator (1 column of 34 cells)

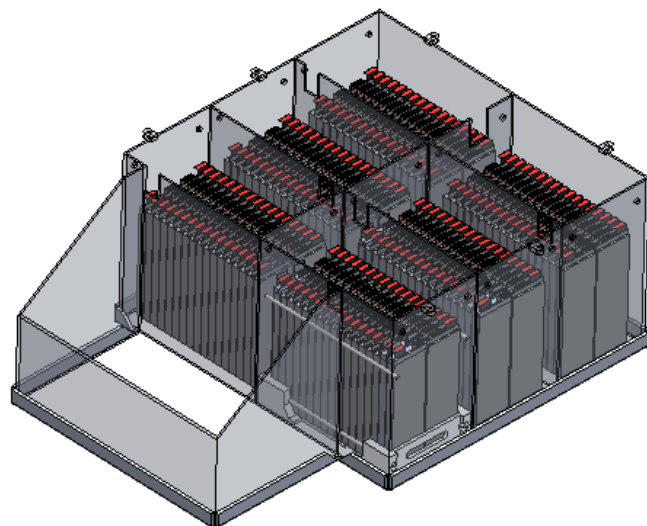


Figure 18: Cell Placement inside Accumulator (2 row of 17 cells each)

Iterations were done to place the cells inside the given space. These were mainly affecting the CG position and were key from a VD point of view.

12. Lid Design

The lid design consisted of two iterations where the lid was considered as a single part in one design and divided in second design the comparison table for the same is given below:

Iteration 1	Iteration 2
Single Piece	2 piece
Direct accessibility to all components	Individual access according to purpose
Faster Disassembly	Slower disassembly for total setup
Easier mounting for better fitment	Difficult mounting for flush fitting
Easier for waterproofing	Difficult for Waterproofing

Table 6: Lid Design Iterations Comparison

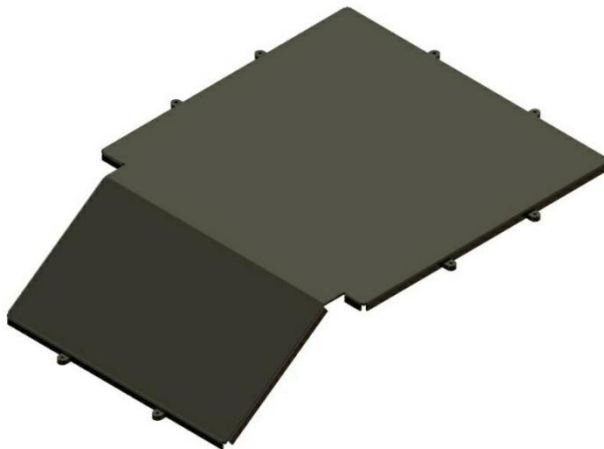


Figure 19: Lid CAD Design

13. Stack Design Flow

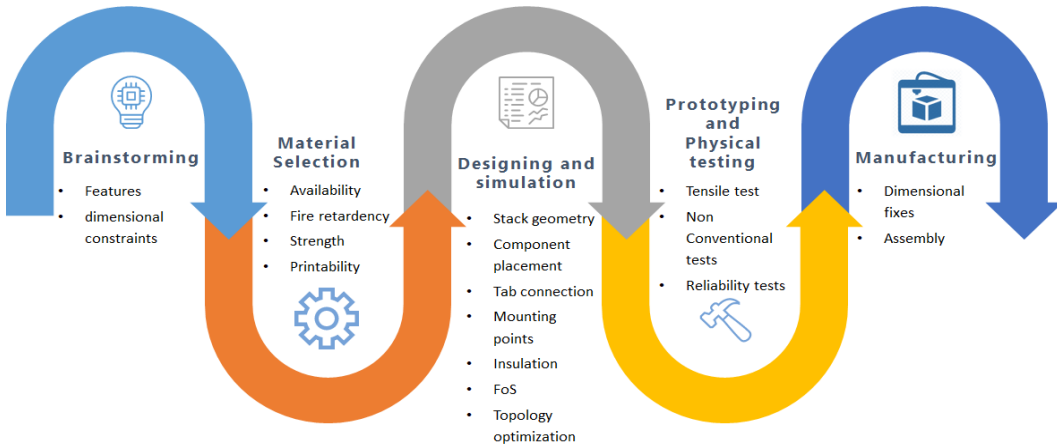


Figure 20: Stack Design Flow

13.1. Stack Iteration – 1

In this iteration the cells were put next to each other. The cell holder design comprises a cross structure for a strong and light product. The major drawback of this design is that the stack is made of aluminium and is not insulated, this makes it unreliable and not preferable. Also, the weight of the segment was quite high as well as had a lot of extra clearances and hence volume.

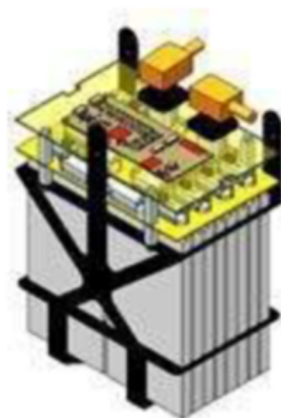


Figure 21: CAD of Stack Iteration - 1

13.2. Stack Iteration – 2

In this iteration the stack was made of FR-ABS, this led to reduce weight to a great extent. We designed it in such a way that it can vary the length to adjust cell pressure. This feature of adjusting cell pressure increased the life of cells. From the graph below, it was studied that light stack pressure is found to be beneficial for long term performance and hence spacer pads were responsible to maintain pressure on the face of cells. These pads maintain enough pressure on the battery pack to ensure secure electrical and thermal connections while allowing the package itself to expand and change shape.

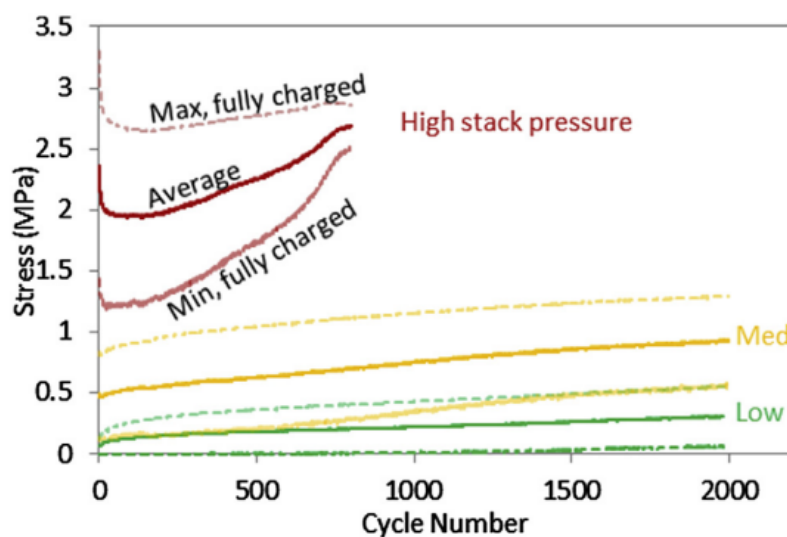


Figure 22: Stack stress evolution as a function of cycle number

The major flaw in this design was busbar arrangement. The distance between busbars in the existing design is 10 mm, however the gap in this iteration was only 2 mm, making it unsafe and difficult to assemble. Furthermore, when compared to existing rectangular busbars, longer busbars add an additional amount of weight.

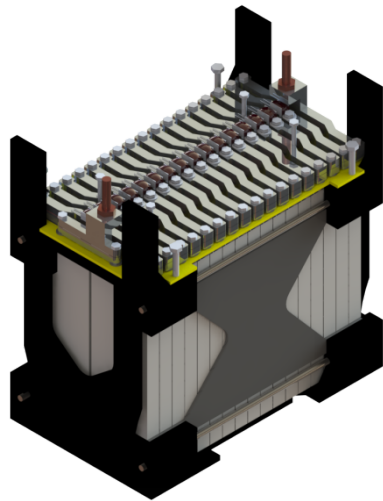


Figure 23: CAD of Stack Iteration - 2

14. Plastic vs Metal Stack

Based on the properties of Metals and Plastic materials we have concluded that the plastic stacks would give us good insulation, and help us with designing and manufacturing in a better way. On the other hand metal stack would have increased the overall weight, and also would have compromised with the insulation of the Accumulator being a good conductor.

Electrical
Insulation



Prototyping
Capabilities



Design
Flexibility



Ease of
Manufacturing



Figure 24: Plastic vs Metal Stack

15. Final Iteration



Figure 25: Final Iteration Stack CAD

Topology optimization was carried out for a set of loads, boundary conditions and constraints to get an optimal structural layout. This helped us reduce weight, cost and manufacturing time of the stack without compromising the mechanical strength.

Simulation of equivalent stress, total deformation and safety factor were performed on Ansys Workbench for three different boundary conditions.

Material properties considered were as below:

Material	Young's Modulus (MPa)	Poisson's Ratio	Tensile Ultimate Strength (MPa)	Tensile Yield Strength (MPa)
FR-ABS (Stack)	1,866	0.3998	29.6	20
Steel (Stud)	2,00,000	0.3	400	250

Table 7: Property data

We tried to achieve detailed mesh for high fidelity simulations.

Mesh details:

Number of nodes - 207850

Number of elements - 107790

Element size - 2 mm

15.1. Boundary condition 1:

Force of 1275.3N (6.5kg x 20 x 9.81) applied at 6 bolt hole points in positive Y direction. Fixed Support at 4 faces at top of stack and diagonally opposite mounting hole points

Boundary Condition 1:

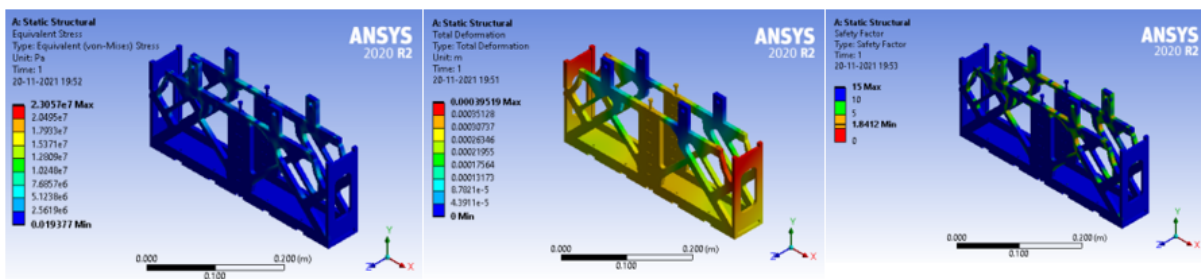
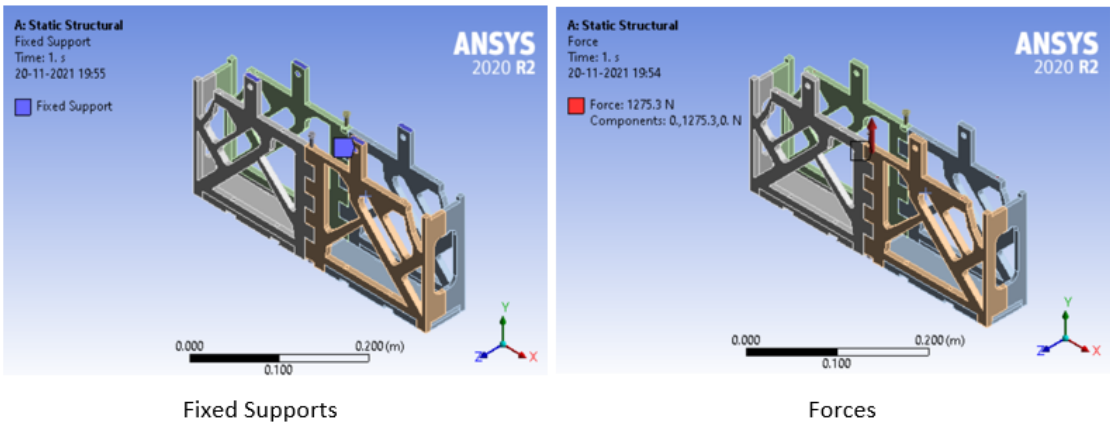


Figure 26: Simulation for boundary condition 1

15.2. Boundary condition 2:

Force of 2550.6N (6.5 kg x 40 x 9.81) applied at face on front side of stack in positive X direction. Fixed Support at front face of side of stack and diagonally opposite mounting hole points.

Boundary Condition 2:

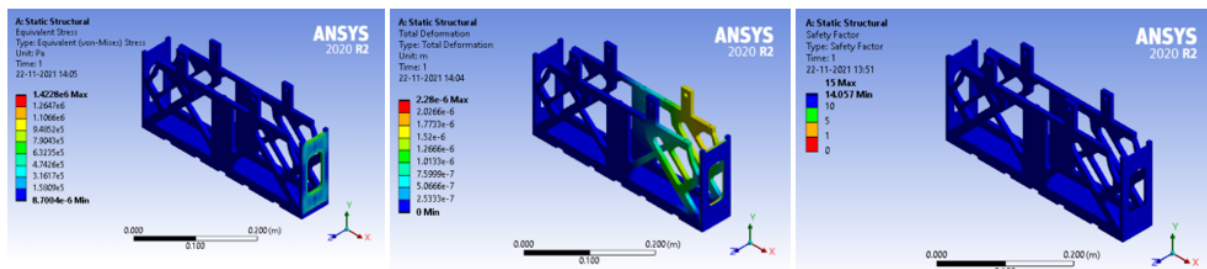
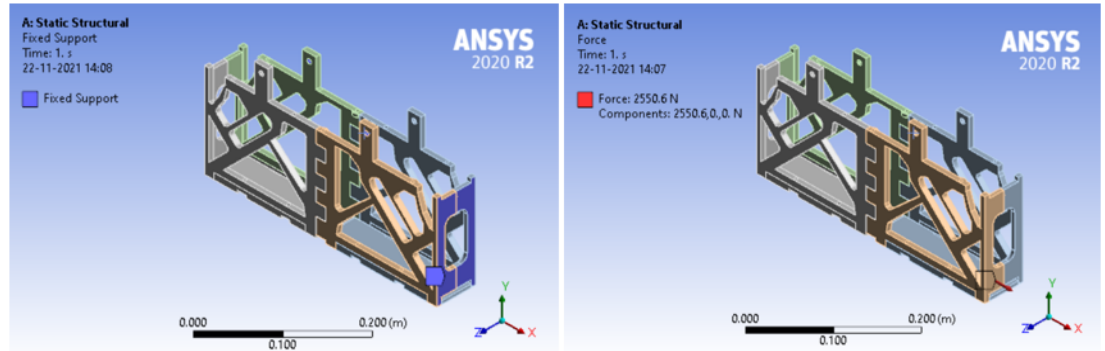


Figure 27: Simulation for boundary condition 2

15.3. Boundary condition 3:

Force of 2550.6N ($6.5 \text{ kg} \times 40 \times 9.81$) applied at face on outer side of stack in positive Z direction. Fixed Support at outer face of side of stack and diagonally mounting hole points.

Boundary Condition 3:

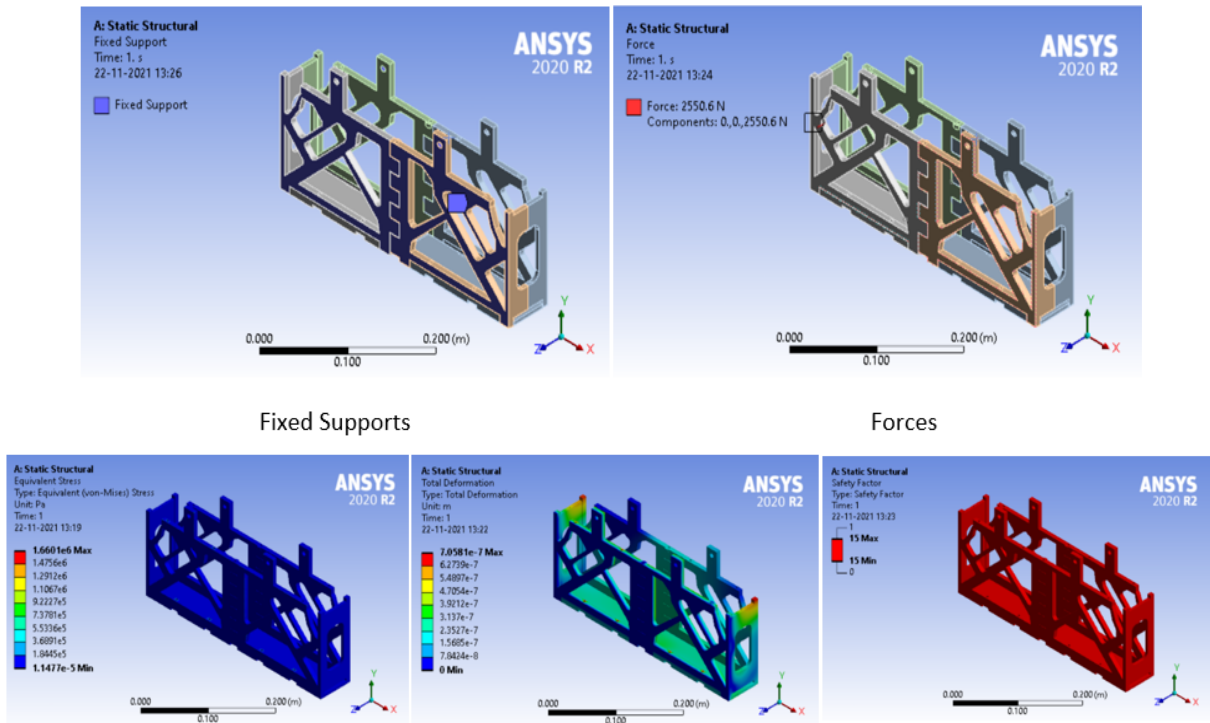


Figure 28: Simulation for boundary condition 3

From the above simulation results, it was clear that the stack is safe and durable, accordingly this design was finalized.

16. Cell Orientation

The cells are placed such that the 2 neighbouring cells have the same polarity. This forms a pair. Such pairs of opposite polarity are placed alternately one after the other to form a connection as shown below.

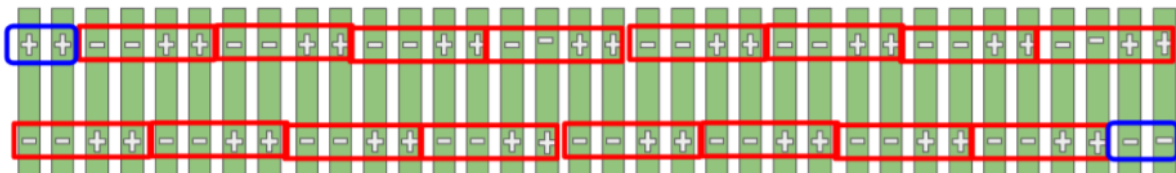


Figure 29: 2p17s Stack Configuration (Busbar Schematic)

17. Separator Design

The segment separators were designed as a jigsaw structure consisting of Al 6063- T6 sheets welded to the accumulator walls. The mounts for each stack were integrated into these separator walls in an alternating pattern for each segment to avoid interdependency between each stack mounting as well as interference. Also, these mounts were placed above the upper AMS holding plate for a safe disassembly process which was quick and convenient.

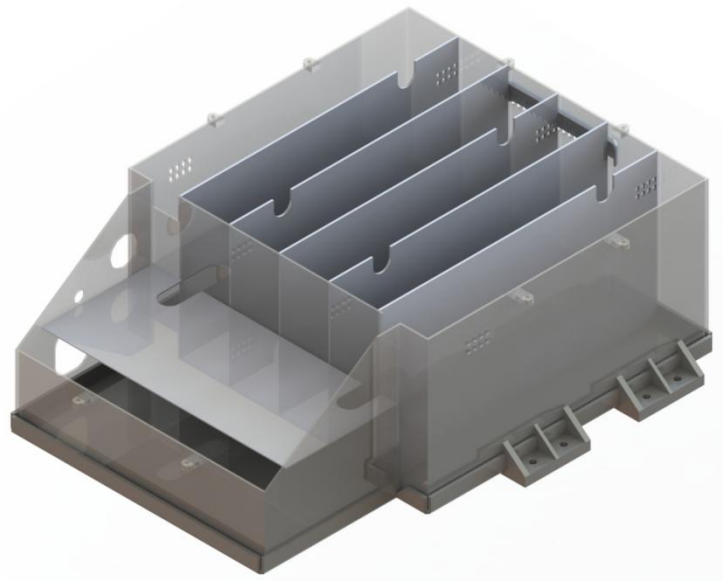


Figure 30: CAD of Separator Placement

18. Stack Orientation

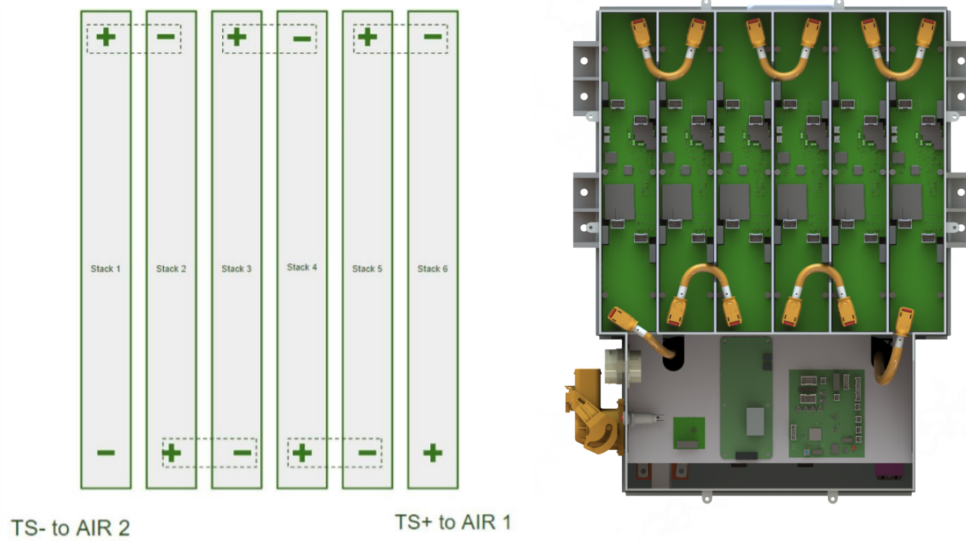


Figure 31: (a) Schematic of electrical connections of 6 stacks (b) CAD rendering of Electrical connection

Each segment extends from front to back in a longitudinal direction. Facing the forward direction, the leftmost stack is the positive most stack and the rightmost stack is the negative most stack. The stacks are named 1 to 6 starting from the negative most stack to the positive most stack.

19. Busbar Design

Before designing the busbar, it was necessary to decide how the connections needed to be made. It was decided to use bolted connections rather than welding for ease of assembly and maintenance. For a bolted connection, we decided to sandwich cell tabs between the busbars and FR-4 sheet. Busbars are mounted with the help of bolts which are threaded into Nutsets in the FR-4 sheet. These are positively locked using tab washers. It was decided to avoid drilling the cell tabs to avoid damaging the cell tabs.

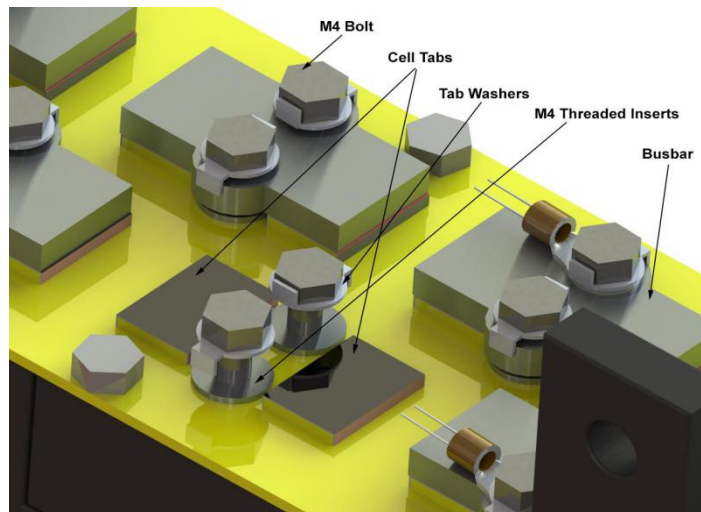


Figure 32: Overlapped Cell Tabs between Busbar and FR4

Material Selection:

To achieve a long and reliable service life at the lowest cost, the conductor material needed to exhibit the following properties:

- Low electrical and thermal resistance
- High mechanical strength in tension, compression and shear
- High resistance to fatigue failure
- Low electrical resistance of surface films
- High resistance to corrosion

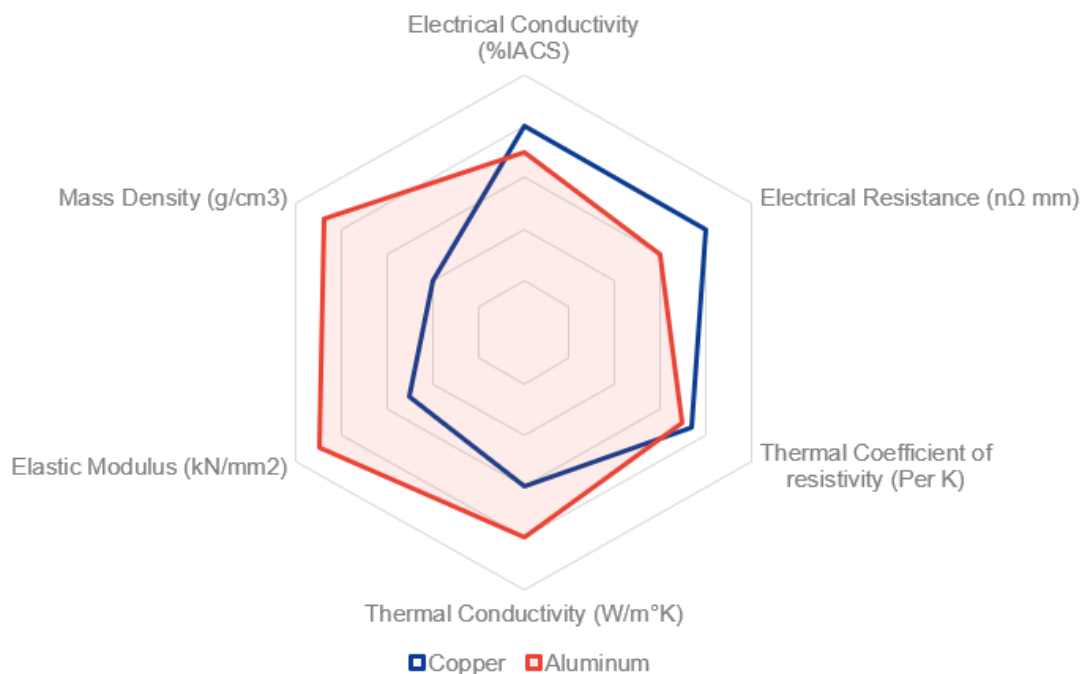


Figure 33: Comparison of Aluminium and Copper

Properties (at 20° Celsius)	Copper	Aluminium	Units
Electrical Conductivity	101	61	%IACS
Electrical Resistance	17.2	23.8	nΩ mm
Thermal Coefficient of resistivity	0.0039	0.004	Per K

Thermal Conductivity	397	230	W/m°K
Elastic Modulus	116-130	70	kN/mm ²
Mass Density	8.96	2.7	g/cm ³

Table 8:Properties of standard grades of copper and aluminium

As seen from the chart, electrical conductivity of copper is higher than aluminium, so an equivalent resistant conductor for aluminium would have a cross-sectional area greater than copper. However, greater hardness of aluminium gives it more resistance to mechanical damage during its range of service. Even though the thermal conductivity of copper is higher than aluminium, the convective heat transfer of aluminium is better than copper, that is, heat dissipation of aluminium is better than copper. Also, the weight of aluminium is nearly three times less than copper.

As most of the current would directly flow through the direct contact of the cell tabs (as cell tabs are made of nickel-plated copper) due to overlapping of cell tabs, and the need for better heat dissipation due to high discharge rates, the material selected for busbars was aluminum.

The heat rejected away from the cells was assumed to be mainly due to forced convection from the busbar. So, it is necessary for maximizing the surface area of the busbar so as to allow maximum contact area with the incoming airflow. The dimensions were restricted due to packaging constraints.

Busbars were designed to have as high thermal mass as possible and provide maximum surface area at the same time. Making solid busbars increased weight but it was negligible as compared to making busbar with fins.

The busbar was made thin and rigid to provide high thermal resistance. A thickness of 4mm was chosen based on current calculations.

Current ratings for rectangular aluminium sections, Grade EIE-M (1350)

Conductor size (mm)	Cross-sectional area (mm ²)	1 bar	2 bars	3 bars	4 bars	5 bars	6 bars
		Approximate ratings (A)					
2.5 × 12	30	118	210	285	360	425	480
16	40	151	275	395	490	580	655
20	50	183	320	450	575	675	770
25	62.5	223	390	540	685	800	910
30	75	263	480	660	840	990	1115
40	100	342	610	860	1080	1260	1425
4 × 12	48	156	290	420	536	620	700
16	64	198	340	470	600	710	815
20	80	238	410	570	720	850	955
25	100	290	530	755	950	1110	1250
30	120	339	600	845	1060	1245	1400
40	160	434	750	1050	1320	1550	1750
50	200	532	905	1260	1575	1825	2035

Figure 34: Busbar Material Ratings

Electrical Power Engineering Reference & Applications Handbook was referred for the table above. Linear interpolation was done by referring to the values, to determine the current rating of a busbar with 57.6mm² cross sectional area. It was determined to be 181.2 A.

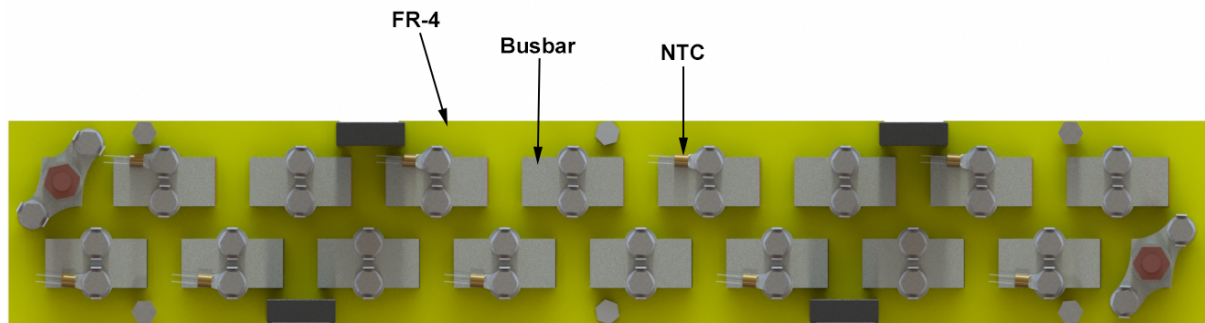


Figure 35: Top View of Stack

After finalizing the dimensions, we can only vary the air velocity for achieving required results. So, we performed a steady state simulation considering heat generated through negative tabs, positive tabs, cell body as 1.7W, 0.7W and 0.4W respectively and it is rejected to the flowing air by the busbar for the complete endurance event for a single cell for various air velocity. It was not feasible to simulate conjugate heat transfer for the entire assembly because of lack of computational power.

20. Mounting Plate Design

The purpose of the mounting plates was as follows:

- A mounting surface for busbars
- Restricting motion of cells
- Electrical isolation
- Holding the AMS and maintenance plugs

FR4 was selected as the material for the mounting plate on the basis of the following parameters:

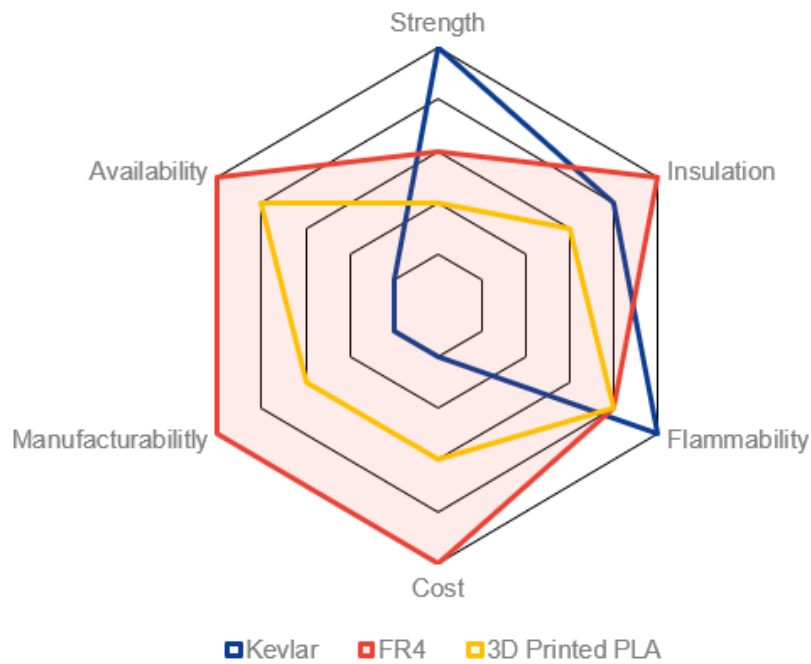


Figure 36: Mounting Plate Selection

21. Final Stack Design

The advantage of flexible and lightweight stack drove us towards the idea of 3D printing. We chose FR-ABS as material for stack because it fitted in our requirements under electrical, mechanical and flame retardant criteria.

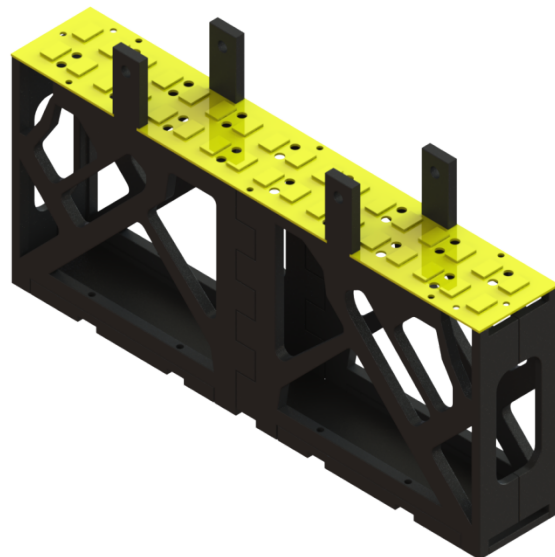


Figure 37: Cell Holder CAD

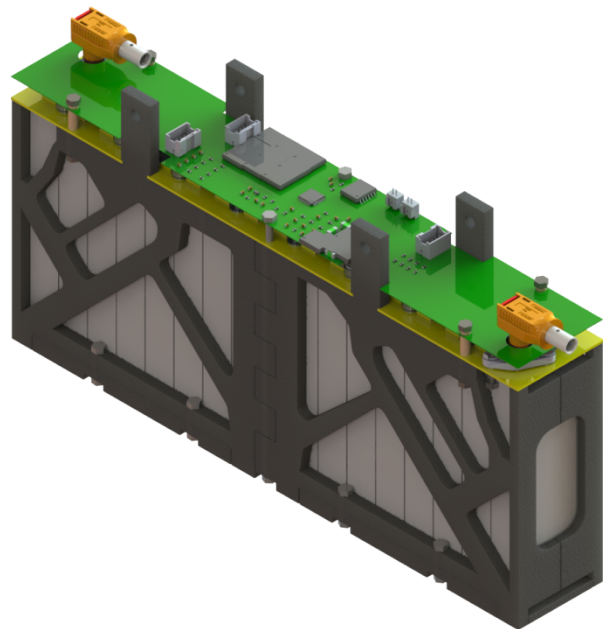


Figure 38: One Stack CAD

22. Insulation

Since the accumulator is a high voltage electrical device, insulation is of utmost importance for the safety of the driver and the engineers working on the vehicle and the battery pack itself. For this purpose, insulating materials were shortlisted on the basis of the following qualities:

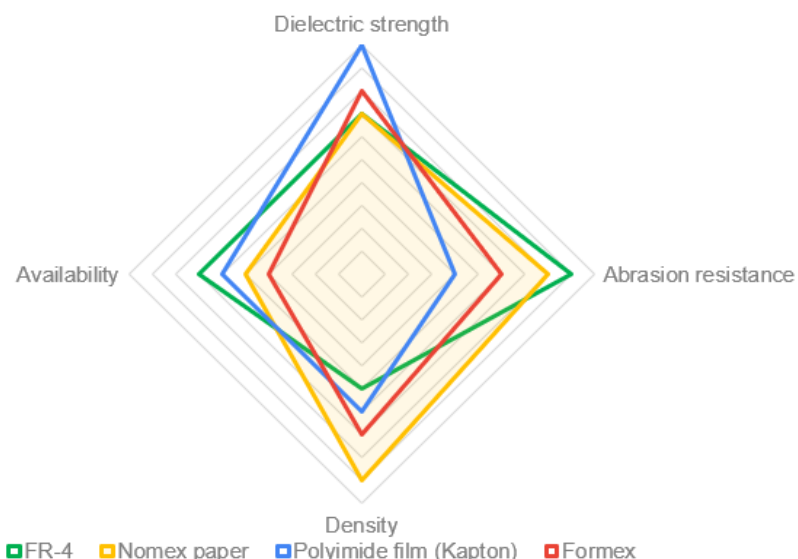


Figure 39: Comparison of Insulation Material

For the stack coverings and busbar and AMS Master mounting plates, FR-4 was chosen as the insulator for its high mechanical strength and high availability and moderate cost.

Nomex paper was chosen as the primary insulation of the accumulator due to its lightweight nature and high abrasion resistance.

Polyimide (Kapton) film was used as a secondary insulator to fill in the gaps in the primary insulator. Formex was not readily available, hence it was not used as an insulator in the system.

23. Manufacturing

23.1. Container

The fixture used for manufacturing the container was made out of milled MDF parts and wooden blocks. These were used to hold the vertical walls in place while welding the structure over which the bottom plate was welded to and then the mounts on the same fixtures. The fixture was made such that it was quick to assemble, and did not affect the accessibility of the welding torch. The accuracy of the machining of these fixtures was ± 0.1 mm while the overall accuracy was slightly lower at ± 0.8 mm.

The accumulator container was manufactured out of Aluminum 6063-T6 sheets which were laser cut. These sheets were further welded in a milled MDF fixture by the use of TIG welding technique. The cell holders also served as a fixture for the welding of containers.

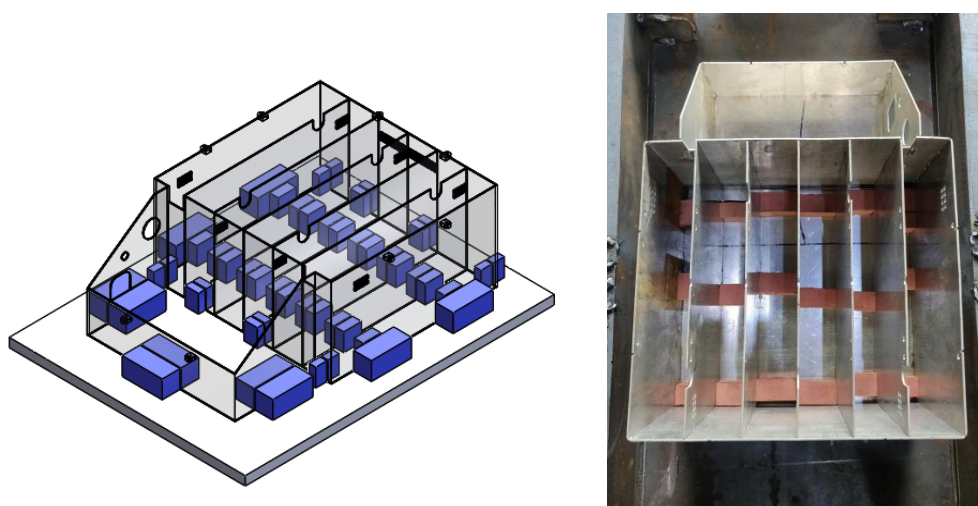


Figure 40: Container Fixture

These fixtures were made in such a manner that the sheets were held in place by blocks of wood fixed in a base plate, such that the welded part could directly be removed without any disassembly and also helped in better accessibility during welding. The base and the lid were bent using CNC bending before welding.

23.2. Busbar Mounting Plates and Accumulator Mounts

FR4 was cut by using milling machine and the accuracy of machining was **±0.05mm** then followed by crimping of nut inserts into them.

The mounts for mounting the accumulator were CNC milled and then welded on the accumulator by using a fixture to improve accuracy.

23.3. Stack

Since the stack was 3D printed, infill percentage played an important role in determining the strength and weight of stack. Accordingly, 50 % infill was set. The stack comprised two parts, the side wall structure and the base. The side walls were manufactured in four parts and base in two parts because of 3D printer bed constraints. We assembled the base and sidewalls using M4 bolts. The dimensional tolerance of 3D printing was **±0.5mm**.

23.4. Assembly

The clearance between internal walls and stack was taken as **2 mm**. This clearance was decided by taking into account tolerances of 3d printing, laser cutting, welding and assembly. The dimensional tolerance of 3D printing of the stack was considered to be **±0.5mm**, the tolerance of laser cutting for the internal walls of the compartment was taken as **±0.2mm**, the tolerance of welding was taken as **±1.0mm** and the assembly tolerance was taken as **±0.3mm** which came to a total tolerance of **±2.0mm**.

The assembly of the cell stack was done in the gravity down approach as illustrated by the following image.

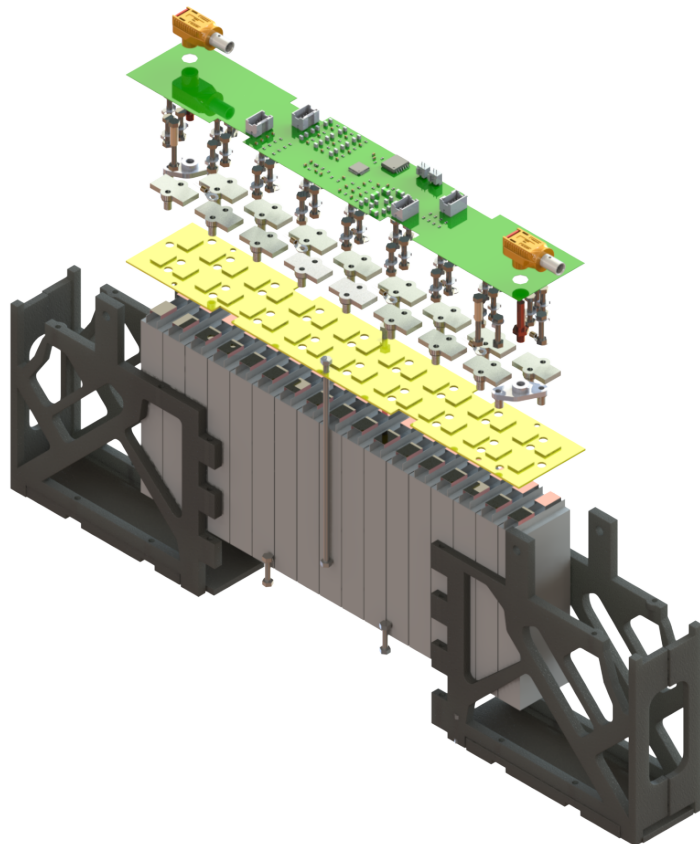


Figure 41: Stack Exploded View

24. Accumulator Management System

24.1. System goal:

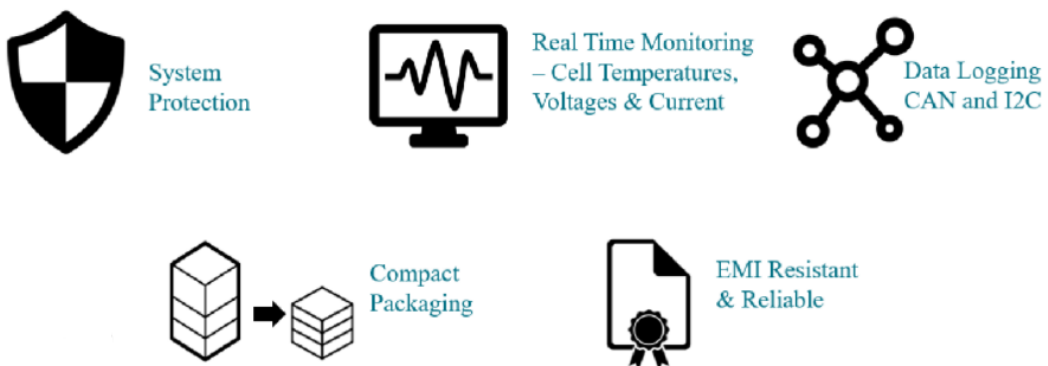


Figure 42: AMS System Goal

24.2. AMS Design.

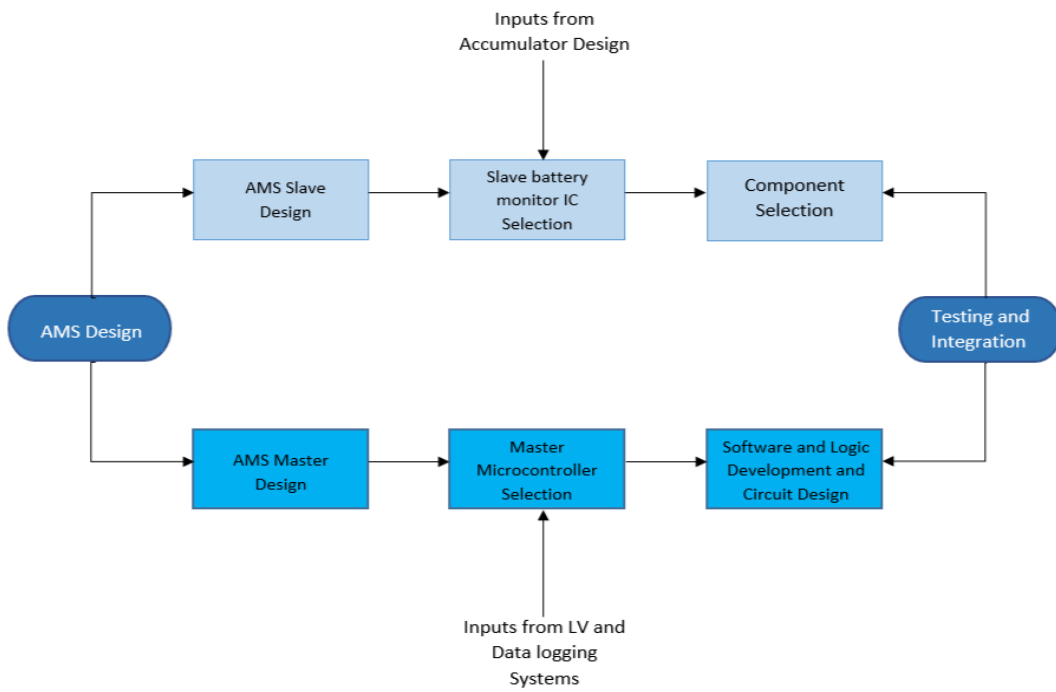


Figure 43: AMS Design Flow

- Each Accumulator Segment has one monitoring board.
- The Slave Boards are Daisy-chained for simplified wiring setup.
- Each Board monitors 17 series cell voltages and temperature of 8 cells.

24.3. AMS TOPOLOGY SELECTION.

The first step in designing an AMS for cell monitoring is to decide the topology of the AMS. The topology selection has a significant impact on the AMS placement and packaging, wiring harness design, and overall design and manufacturing process of the accumulator container. Hence, topology selection plays a vital role in AMS design.

Three different topologies for an AMS are: Distributed, Modular and Centralized. In Distributed topology, there are small voltage and discharge monitor circuits which communicate with the master controller of the AMS. In Modular Topology, multiple slave BMS controllers are used to fetch the data and forward it to the master controller. In Centralized topology, the Centralized master controller is directly connected to each cell of the battery pack, the controller unit protects the cells.

Each topology has its own advantages and disadvantages in design, manufacturing and assembly. These are listed in the table below. Each Parameter is given a number between 1-5, with 5 representing best and 1 representing worst.

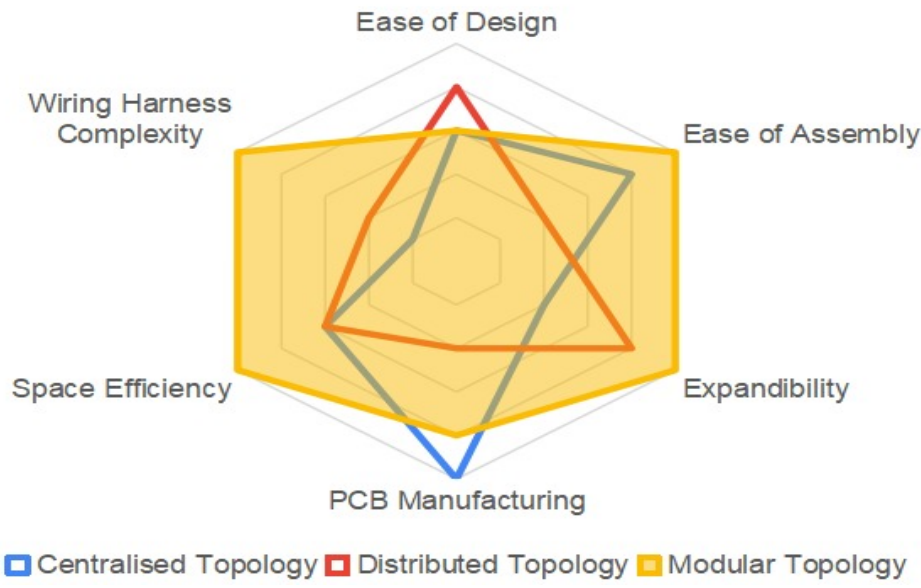


Figure 44: AMS Topology Selection

From the table, it is clear that the Modular topology offers several advantages over other designs. It has the simplest wiring harnesses of all, is the easiest to assemble, has excellent space efficiency and has the capability to easily expand to handle a larger or smaller number of cells. Thus, it is evident that the Modular Topology AMS was the best choice for our requirements.

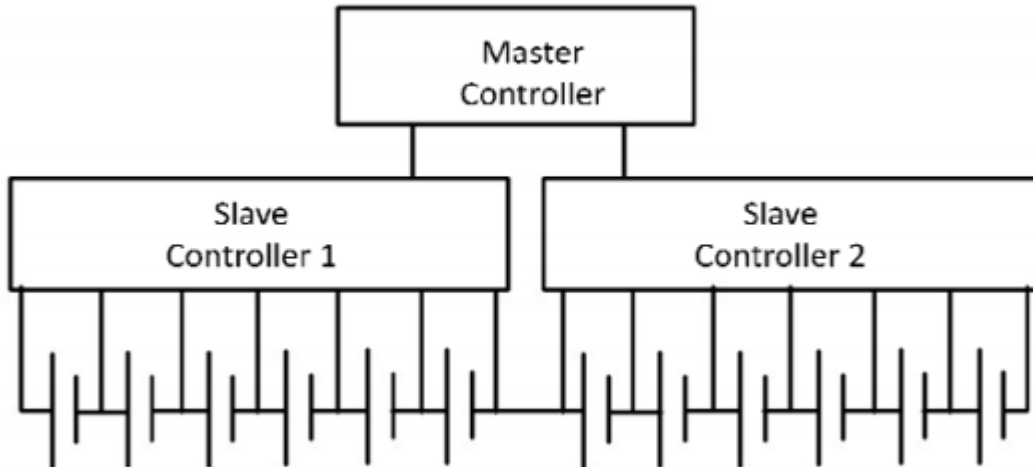


Figure 45: Modular AMS Topology

24.4. Slave IC Selection

To select the best IC for our needs, we performed market research and explored the different options offered by various semiconductor manufacturing companies. The shortlisted products, their parameters and features are listed in the table below:

Manufacturer	Maxim Integrated	Linear Technologies		Texas Instruments	NXP	STMicroelectronics
Part No	MAX14920	LTC6804	LTC6813	BQ76PL455	MC33771	L9963E
Number of Cells Monitored	Up to 12	Up to 12	Up to 18	Jun-16	!4	Apr-14
Number of Temperature Sensors	3	6	9	8	8	7
Communications with Master Controller	4 Wire SPI	2 Wire isoSPI	2 Wire isoSPI	2 Wire UART	2 Wire Iso SPI	4 Wire SPI

Table 9: AMS Slave Monitoring IC Selection

From the above table, the LTC6813 was selected since it could monitor the highest number of cells, 18. It also allows us to design an AMS Slave board PCB with only one monitoring IC, simplifying the design procedure as well as reducing the size and cost of the board. The LTC6813 also features a 2 wire isoSPI interface, which provides daisy-chaining functionality and high noise immunity using galvanically isolated differential pair for communication. Its stackable architecture allows virtually unlimited numbers of boards to be connected in series to monitor large numbers of cells. The LTC6813 also features 9 temperature sensor inputs in order to monitor temperatures of cells across the pack.

The LTC6813 is also supported by Linear Technologies' Linduino Program and has libraries available for programming the IC. This greatly simplifies the software development process and improves the reliability of the final firmware.

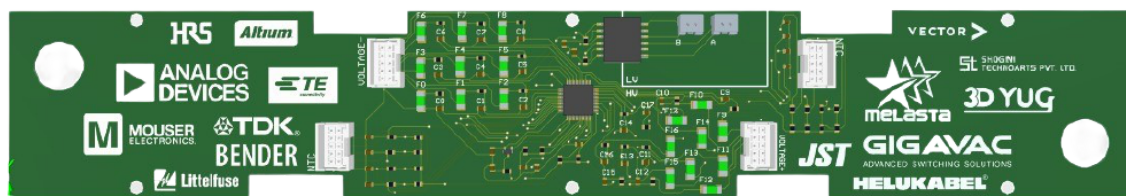


Figure 46: Slave PCB

24.5. Master IC Selection

The AMS Master is the main controller of the Accumulator Management System. It is responsible for executing the cell voltage and temperature monitoring functions, calculating fault conditions and transmitting data externally to the data logging unit. Hence, the AMS Master must incorporate a high-performance, easy to program microcontroller unit (MCU). The MCU must be fast enough to handle the fault conditions within the stipulated time period while simultaneously handling monitoring and logging functions.

With these factors in mind, we researched and considered different microcontroller families to find the best one suited to the task. The researched data is presented in the following table:

Architecture	AVR	PIC	ARM Cortex M0+, M3 or M4
Families	AtMega Series	PIC16,PIC18, PIC32	STM32,MSP432P4011T
Ease of Programming	Very Easy	Intermediate	Intermediate
Library Support	Very Good	Low	Moderate
Clock Rate	16 MHz	16 MHz	48 Hz and Greater

Table 10: AMS Master IC Selection

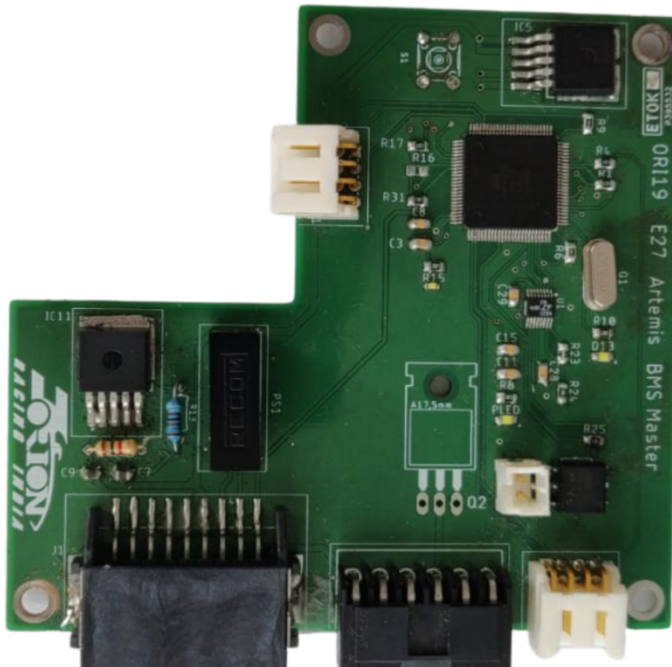


Figure 47: Master PCB

Due to ease of programming, a great library and community support, low cost and easy availability, the AVR family of microcontrollers was selected. In particular, the AtMega 2560 MCU was selected for its large program memory size of 256KB and Arduino community support, which included support for all the peripherals present in the MCU, plus a multitude of external peripherals as well.

Each AMS board sensed 17 cells placed in series. 6 such boards are daisy-chained to monitor a total of 102 cell voltages. The Cell voltage and temperature values are sent to the AMS master from the AMS slave boards through isoSPI, to provide noise immunity. The communications wiring uses transformers at each end for galvanic isolation between the boards. Differential signaling is employed to maintain signal integrity in high EMI situations.

The AMS Master continuously checks if any of the parameters are outside of the permissible limits according to the rules. If the specified limits of both values, as well as time, are exceeded, the AMS issues a fault signal which is transmitted to the Shutdown Circuit, which then opens the AIRs to cut off the accumulator from the rest of the vehicle. A red indicator light present in the cockpit marked with the lettering “AMS” which lights up if the AMS opens the shutdown circuit and stays illuminated until the error state has been manually reset.

24.6. Data Flow through the Accumulator Management System.

The AMS master continuously monitors all the cell parameters .These values are sent to the data logger using CAN bus. We experienced unusual voltage drops in particular cells during the test runs and thus with the help of our data logger we were able to get to the root cause of the issue and thus clarify the same.

We have also logged the max DC power consumed during our runs. This data helped us in estimating the maximum power that is consumed in endurance and acceleration runs with different settings of motor parameters and allowed us to abide by the rules and also extract maximum output from the powertrain system.

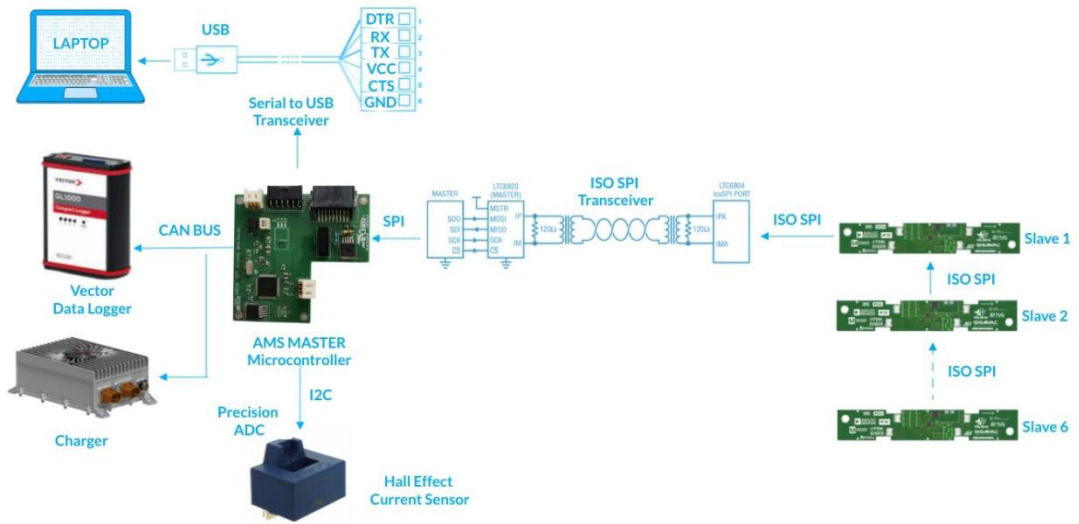


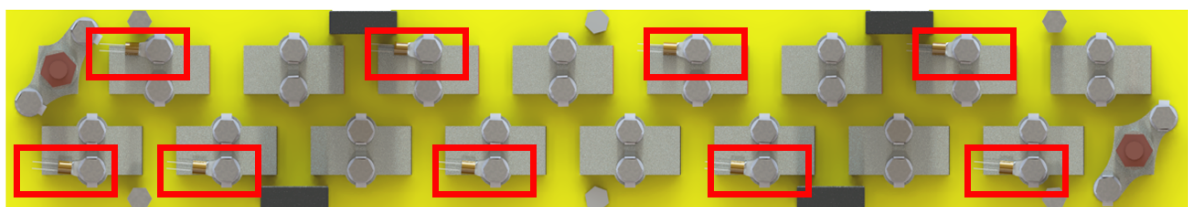
Figure 48: Data flow diagram

24.7. Cell temperature monitoring:

For measuring the temperature of the cells Negative Temperature Coefficient (NTC) type Thermistors is used which has a resistance of 10K ohms at 25 degrees Celsius with a Beta value $3988 \pm 1\%$

Position: 8 sensors are spaced throughout a 2p17s segment resulting in 47.05% of cells being monitored in the accumulator container. The distance between the two negative cell tabs on the busbar and the NTC thermistor temperature sensor is less than 10mm hence monitoring both cells connected to the busbar.

Thus, there are overall 48 temperature sensors across the accumulator that are used for monitoring the temperature of the cells continuously.



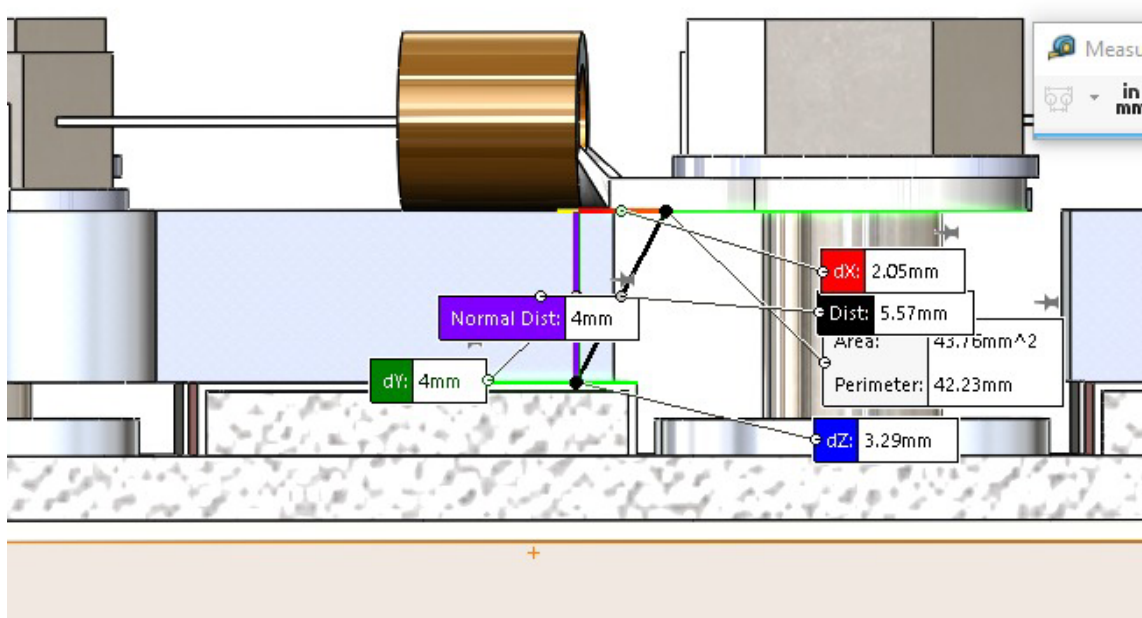


Figure 49: NTC Placement

24.8. AMS Logic Flow Diagram

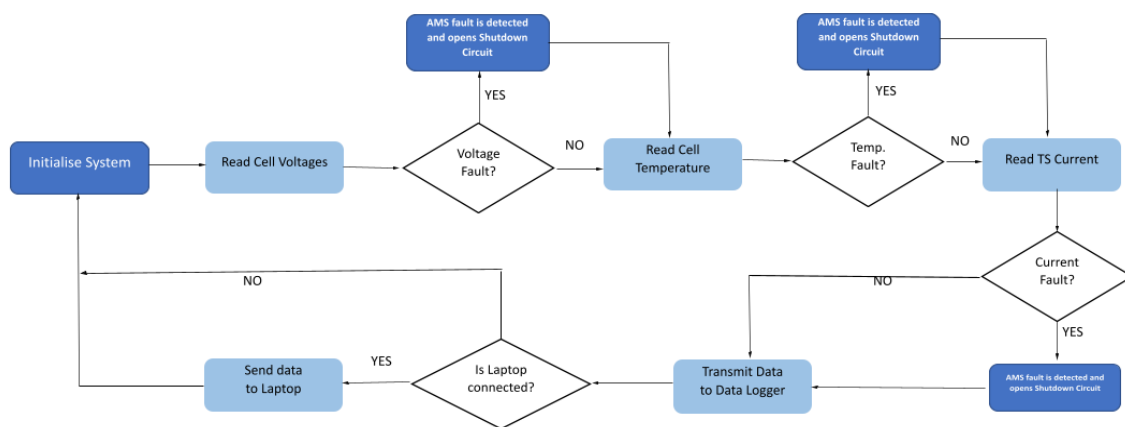


Figure 50: AMS Logic Flow Diagram

24.9. Model and SoC Estimation:

The purpose of designing a battery model is to provide a way to estimate or predict the performance of the battery cell before manufacturing, assembling and testing the battery pack, as well as assist in implementing an accurate State of Charge Estimation algorithm. This model will help us during the design and testing phase of vehicle development, and assist in selecting the optimum cells for our application based on the lab test data for the respective cell. The cell model can be integrated with the other vehicle subsystem models to provide additional information such as the heat generation of the cells during use.

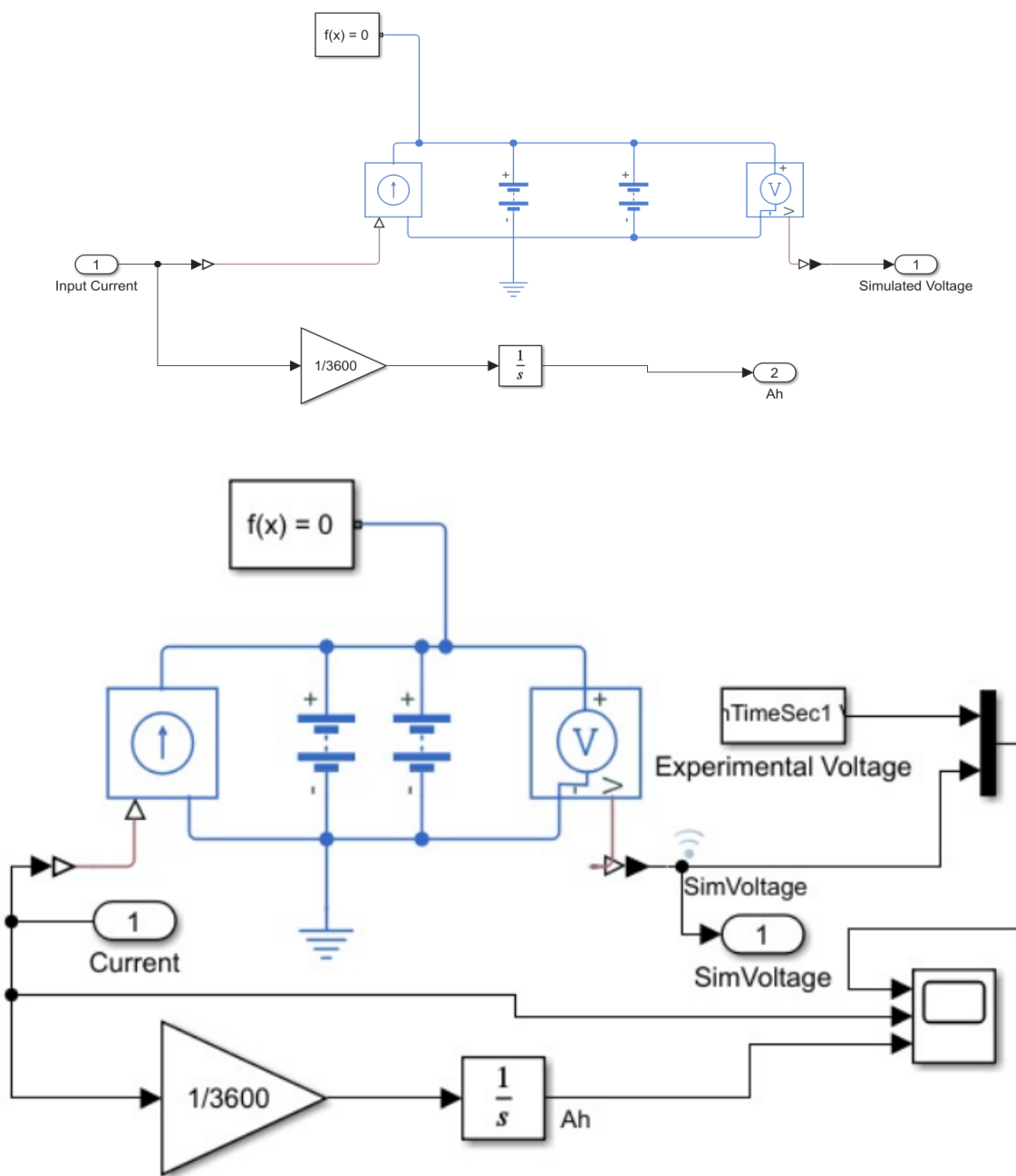


Figure 51: Simulink Model

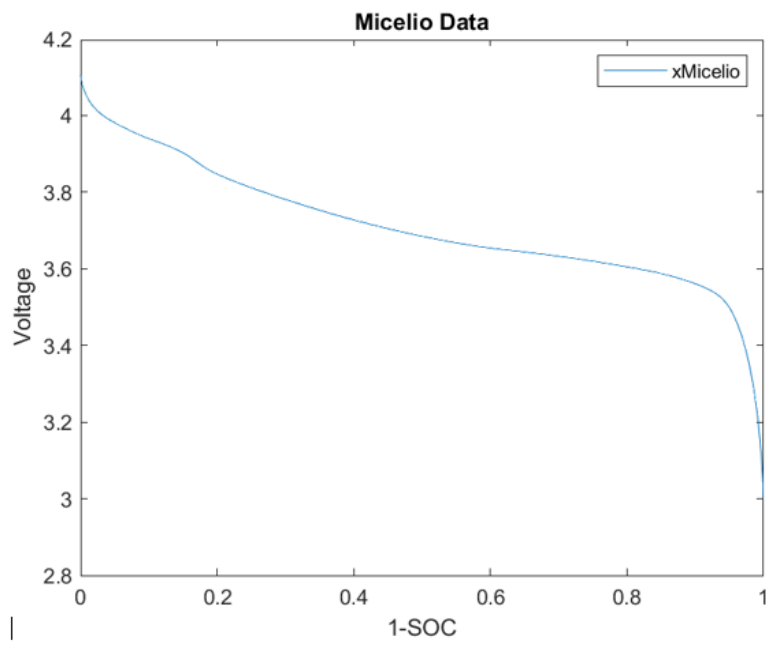


Figure 52: SOC Curve

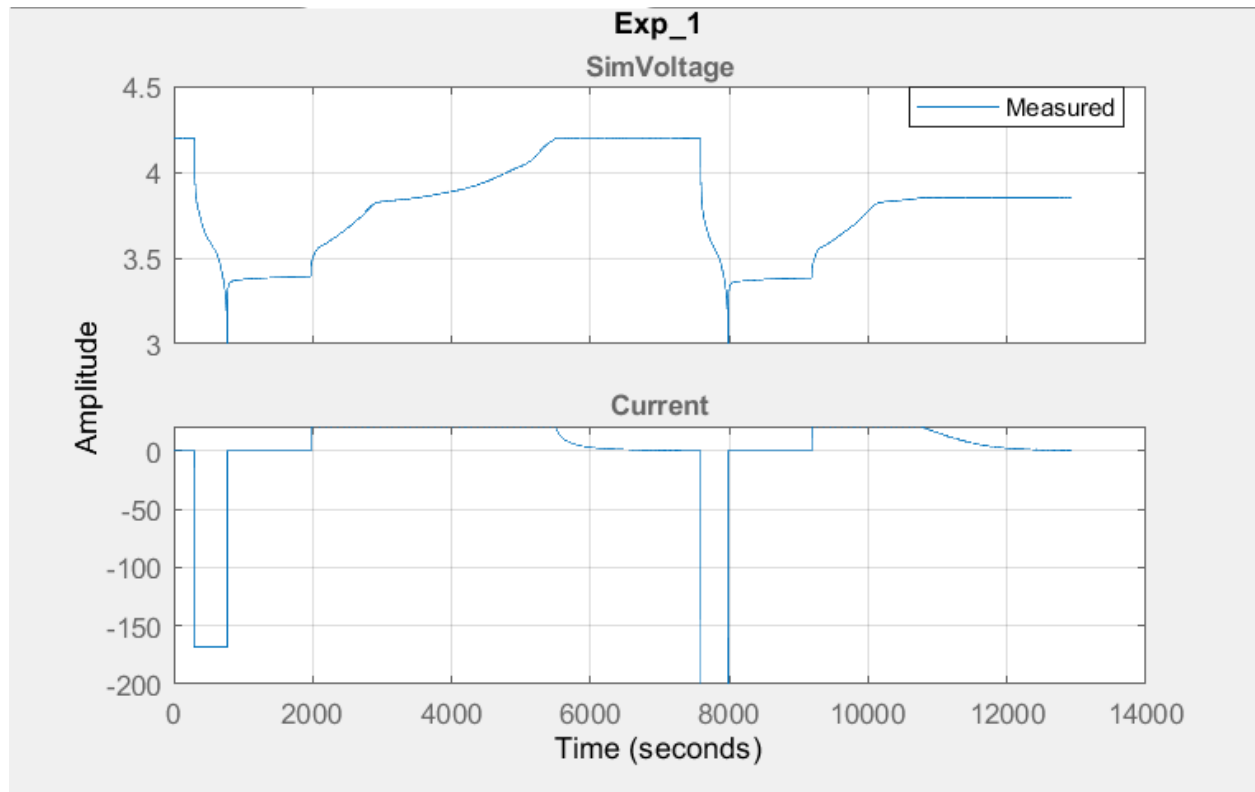


Figure 53: Simulation Graph

A cell model testbench was developed in Simulink as shown in the figure. A 2 RC pair Equivalent Circuit Cell Model was selected to balance the accuracy of cell dynamic response with the parameter estimation

complexity. The model was parameterized and RC values found using Simulink Design Optimization tools. This tool gave us the vectors of R and C values as a function of SoC.

Using the cell model parameters, an SoC estimation algorithm is proposed using a model based state estimation algorithm. Currently, we are evaluating two approaches for the state observers, which are the Kalman Filter (and its extended and unscented variants) and the Luenberger Observer. The Kalman Filter has its advantages in robustness, since it considers the noise covariances of the sensors used in the BMS. On the other hand, the Luenberger Observer offers faster performance and easier deployment due to its relative simplicity. However, it does not take into account the sensor noise covariances, and thus will not be as robust as a Kalman Filter implementation under heavily noisy conditions. Thus, we are evaluating both methods for SoC estimation and will select the best method that provides the desired accuracy with the least implementation effort.

25. Wire Model

A Simulink model was developed based on the above algorithm to determine heat generated due to current travelling in wires. This helped calculate the temperature deltas and wire temperatures for a given current value. Based on that an optimal wire size was decided.

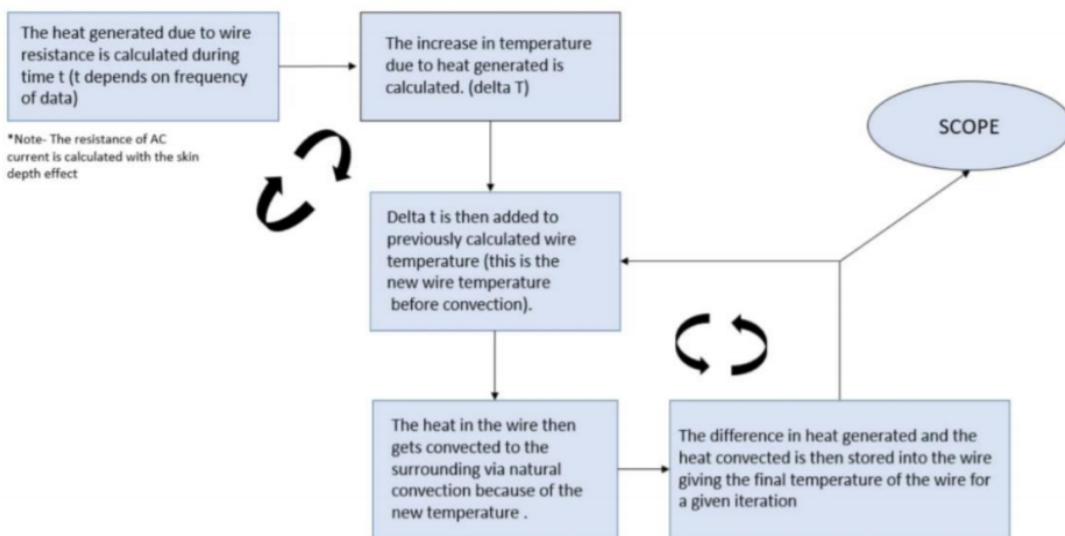


Figure 54: Wire Model Flowchart

Input (Wire specification):

1. Radius of wire
2. Cp of insulation material
3. Density of insulation
4. Volume of insulation

5. Outer Area of insulation
6. Conductivity of wire
7. Length of wire

Current, frequency = $f(t)$

Environmental Constant-

1. Ambient temperature
2. Convective heat transfer coefficient ($8 < H < 14$) (assumed)

Formulas-

$$\text{Heat generated} = I^2 RT$$

$$\text{Increase in temperature} = \frac{\text{Heat}}{\text{Thermal mass of insulation (mCp)}}$$

$$\text{Heat liberated convection} = H * A * (T_{\text{wire}} - T_{\text{ambient}})$$

$$\text{Heat to be stored in wire} = \text{Heat generated} - \text{Heat liberated}$$

$$\text{Skin depth} = \frac{0.066}{\sqrt{f_{\text{current}}}}$$

$$\text{Resistance} = \text{length of wire} / \text{Equivalent area of wire for conduction} * \text{Conductivity}$$

Output – Temperature of wire v/s time:

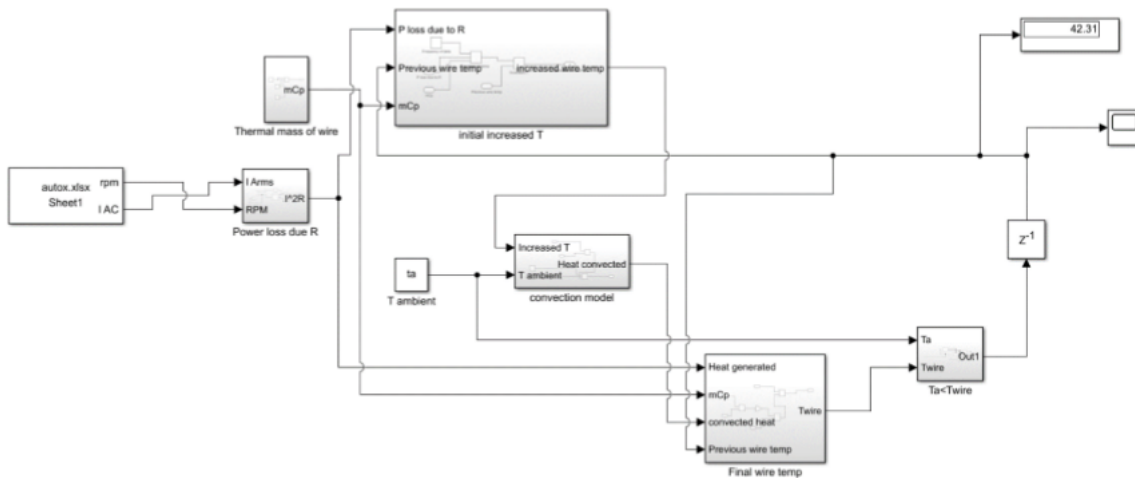


Figure 55: Simulink Wire Model

25.1. Model Verification:

In order to test the model's dependency, a Polycab single core HV wire was tested for constant load current at a nearby testing facility.

The results are as follows

Cross section	25	mm ²
Major Radius	6	mm
Length	1000	mm
radius of wire	2.820947918	mm
Area of surface	0.037699112	m ²
Volume of insulation	8.80973E-05	m ³
density of insulation	1450	kg/m ³
mass of insulation	0.127741137	kg
Metal density	8890	kg/m ³
Volume of metal	0.000025	m ³
weight of metal	0.22225	kg
Cp of insulation	1300	j/kgK
Cp of metal	385	j/kgK
M*cp metal	85.56625	j/k
M*cp of insulation	166.0634775	j/k
total	251.6297275	j/k
Resistance per mm	0.000000727	ohm/mm
Resistance	0.000727	ohm

Figure 56: Input Parameters

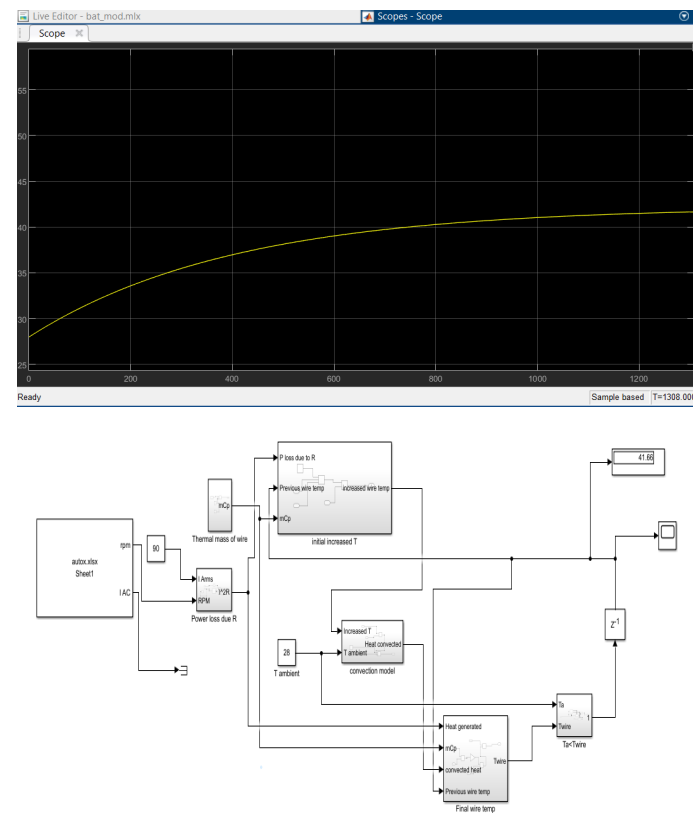


Figure 57: Working Model for 25mm squared wire

26. HV Components

26.1. TS Fuse

For selecting the fuse based on the system requirements a table was prepared which listed the Continuous Current Rating of the components . This table helped in determining the minimum continuous rating the fuse should have and thus Littelfuse - L50QS100 was chosen which has a current rating of 100A

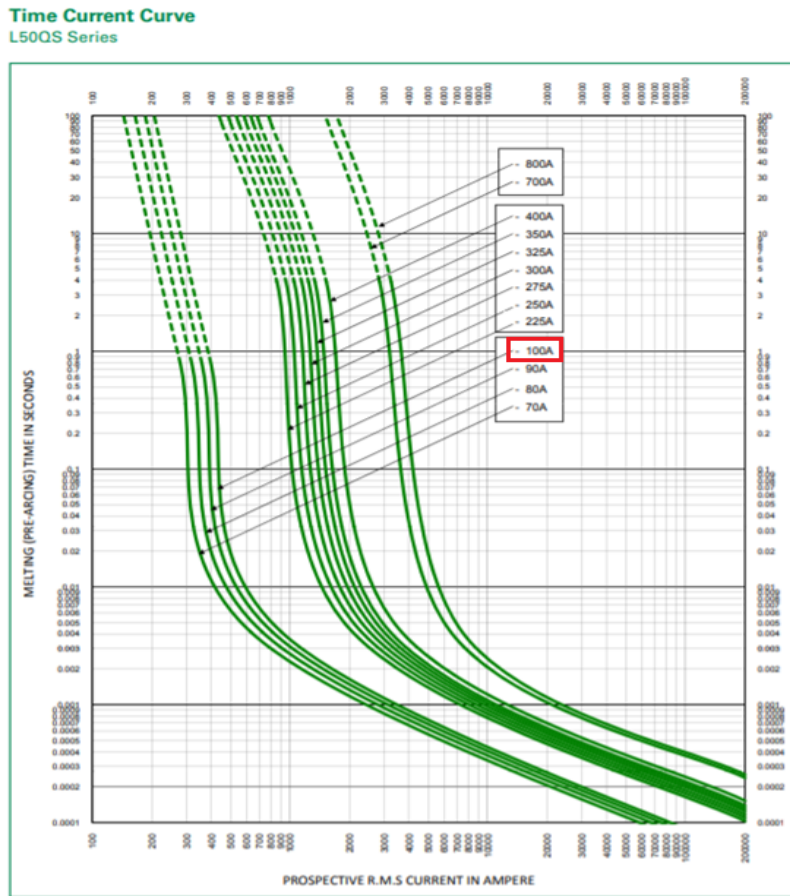


Figure 58: TS Fuse Datasheet

26.2. HV Cables

Through Lap simulations that were performed, it was observed that the RMS current drawn from the accumulator was approximately 80A and peak current drawn from the accumulator was 224.4A for a maximum duration of 2.1 seconds. Cables from Helukabel of 25sq.mm for connections between Accumulator to HVD ,HVD to motor controller , Cell Segment connections to maintenance plugs inside accumulator were selected and 35sq.mm for connection between motor controller to motor were selected.

Technical data	
• Special PVC single core cable acc. to UL-Style 10107 and CSA AWM I/II A/B, core acc. to DIN VDE 0285-525-2-31 / DIN EN 50525-2-31 (except 300 mm ²)	
• Temperature range flexing -5°C to +90°C fixed installation -40°C to +90°C	
• Permissible operating temperature max. +90°C at conductor	
• Nominal voltage VDE U ₀ /U 600/1000 V UL/CSA 600 V	
• Test voltage 4000 V	
• Breakdown voltage min. 8000 V	
• Insulation resistance min. 20 MΩ/km	
• Minimum bending radius flexing 7,5x cable Ø fixed installation 3x cable Ø	
• Coupling resistance max. 250 Ohm/km	
• Radiation resistance up to 80x10 ⁶ cJ/kg (up to 80 Mrad)	

Cable structure	
• Bare copper, extra fine wire conductors, to DIN VDE 0295 cl.6, col. 4, BS 6360 cl.6 and IEC 60228 cl.6, however by 185 mm ² up to 300 mm ² with reduced single wire-Ø, max. 0,30 mm	
• Core insulation of special PVC compound type T13 to DIN VDE 0207-363-3 / DIN EN 50363-3 and class 43, 90°C acc. to UL-Std. 1581 colour black or green-yellow	
• Tinmed copper braided screening, coverage approx. 80%	
• Outer sheath special PVC compound type YM5 to DIN VDE 0207 part 5 and class 43, 90°C acc. to UL-Std. 1581	
• Sheath colour black (RAL 9005) • with meter marking	

Properties	
• Chemical Resistance - see table Technical Informations	
• Resistant to mineral oils, synthetic oils and lubricating coolants.	
• The materials used in manufacture are cadmium-free and contain no silicone and free from substances harmful to the wetting properties of lacquers	
Tests	
• PVC self-extinguishing and flame retardant acc. to DIN VDE 0482-332-1-2, DIN EN 60332-1-2, IEC 60332-1 (equivalent DIN VDE 0472 part 804 test method B), UL VW-1, CSA FT1	
• Acc.to UL-Style 10107/ UL-Std.1581, CSA C22.2 No 210	

Note	
• G = with green-yellow conductor	
x = without green-yellow conductor (OZ)	
• 300 mm ² in adaption	
• AWG sizes are approximate equivalent values. The actual cross-section is in mm ² .	
• non screened analogue type:	
Single 602-RC-J/O	

Nominal cross-section	Group 1		Group 2		Group 3	
	power rating	protective fuse	power rating	protective fuse	power rating	protective fuse
mm ²	A	A	A	A	A	A
0,05	1	-	1	-	2	-
0,14	2	-	2	-	3,5	-
0,25	4	-	4,5	-	6	-
0,34	6	-	6	-	9	-
0,5	9	-	9	-	12	-
0,75	12	-	12	10	15	10
1	15	10	15	10	19	16
1,5	18	16	18	16	24	20
2,5	26	25	26	25	32	25
4	34	25	34	25	42	35
6	44	35	44	35	54	50
10	61	50	61	50	73	63
16	82	80	82	63	98	80
25	108	100	108	80	129	100
35	135	125	135	100	158	125
50	168	160	168	125	198	160
70	207	200	207	160	245	200
95	250	250	250	200	292	250
120	292	250	292	250	344	315
150	335	315	335	315	391	355
185	382	355	382	355	448	400
240	-	-	453	425	528	500
300	-	-	523	500	608	600
400	-	-	-	-	726	630

Figure 59: Helu Kebel 25mm² datasheet

26.3. Maintenance Plugs

The maintenance plug used is Amphenol – Radlok – 5.7. The maintenance plugs allow for rapid assembly and disassembly of the accumulator pack as they can be easily detached or attached.

Pin Type	Pin End	RADLOK™ Pin Size (mm)	Current (A)	RADLOK™ Dimensions(mm)												
				C	D	E	G	L	M	N	P	Q	S	W	Thread	Torque Force (N·m)
Pin	N/A	3.6	70	28.0	7.0				17.5	N/A	8.0				M4x0.7-6g	2.5±0.2
		5.7	120	34.1	10.0				21.1	10.0					M6x1.0-6g	4.0±0.4
		8.0	200	42.4	13.0	N/A	N/A	N/A	26.4	12.0	N/A	N/A	N/A		M8 x 1.25-6g	7.5±0.5
		10.0	300	53.2	16.0				32.2	16.0					M10 x 1.5-6g	20.0±1.0
		12.0	400	58.6	18.0				32.6	20.0					M12 x 1.75-6g	24.0±1.0
		14.0	500	72.0	24.0				41.0	23					M14 x 2.00-6g	24.0±1.0

Figure 60: Maintenance Plug Datasheet

26.4. Current Sensor

The AMS continuously measures the TS current using the current sensor from the LEM HAS series. It is based on Hall Effect technology. This sensor is capable of bidirectional current measurement. It outputs a differential voltage of up to 4V which corresponds to the current of 200A nominal current.



Figure 61: Current Sensor

26.5. Accumulator Isolation Relays

The AIRs used are single pole single throw normally open GIGAVAC – GV241BAB relays rated for 400 amps continuous current. These insulation relays are used between the negative and positive battery terminals before the high voltage motor controller

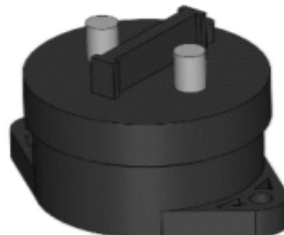


Figure 62: Accumulator Isolation Relay

26.6. Temperature Sensor

The sensor used for measuring temperature of cells is a Negative Temperature Coefficient (NTC) type Thermistor by TDK. The nominal resistance of the thermistor is $10\text{K}\Omega$ with a Beta value of 3978.



Figure 63: Temperature Sensor

27. Future Scope

The future scope for the accumulator from a mechanical standpoint appears to be very good. Many new materials and manufacturing methods can be used to improve the system and make it lighter, and more optimized. The container can also be made from lightweight composites infused with insulating and flame-retardant resin to ensure greater safety. GFRP, CFRP and Aramid fibres are suitable candidates for the container, lid and separator walls.



Figure 64: Composite Accumulator

There are many exciting new technologies that can be implemented in the future into the system and we are enthusiastic for what the future holds for engineering the system better.